WADC TECHNICAL REPORT 54-383
PART I
ASTIA DOCUMENT NUMBER AD-97323

SHOCK-TUBE FLOW INVESTIGATIONS

PART 1 AN EXPLORATORY STUDY OF THE GENERATION OF BLAST-TYPE PROFILES IN THE SHOCK TUBE BY THE REFLECTION METHOD

Robert C. K. Lee
J.Ray Ruetenik
Emmett A. Witmer

MASSACHUSETTS INSTITUTE OF TECHNOLOGY

1 AUGUST 1956

AIRCRAFT LABORATORY
CONTRACT NO. AF33(038)-8906
PROJECT NO. 1350

WRIGHT AIR DEVELOPMENT CENTER
AIR RESEARCH AND DEVELOPMENT COMMAND
UNITED STATES AIR FORCE
WRIGHT-PATTERSON AIR FORCE BASE
DAYTON, OHIO

FOREWORD

This report was prepared at the Aeroelastic and Structures Research Laboratory, Massachusetts Institute of Technology, Cambridge, Massachusetts, on Air Force Contract AF33(038)-8906, under Project Number 1350, (U) "Atomic Weapon Effects on Aircraft Systems." The work was administered under the direction of the Structures Branch of the Aircraft Laboratory, Wright Air Development Center, with Mr. Francis J. Janik, Jr., acting as project engineer.

A series of reports, of which this is Part 1, on theoretical and experimental studies of shock-tube flows will appear as component parts of WADC TR 54-383, (U) "Shock-Tube Flow Investigations."

The cooperation of Mr. Janik and his WADC staff during and since development of the shock tube facility is appreciated. Professor R. L. Bisplinghoff and Professor J. W. Mar directed these studies; their advice and guidance is gratefully acknowledged. The entire staff of the MIT Aeroelastic and Structures Research Laboratory has been most cooperative. The authors wish particularly to thank Mr. George Reitano and Mr. Eugene DiFrancesco who assisted in conducting the experiments and making the measurements. Finally, the figures were prepared by Mr. John McHugh and Mr. George Falla. The text was typed by Mrs. Barbara Marks and Miss Kathryn Roberts.

ABSTRACT

Examination is made of the blast-type profiles which can be produced in the shock tube by the reflection method, and their characteristics are discussed. The feasibility of using this blast-profile generation method for routine shock tube testing purposes is indicated.

PUBLICATION REVIEW

This report has been reviewed and is approved.

FOR THE COMMANDER:

E. H. Schwartz

for Daniel D. McKee
Colonel, U.S.A.F.
Chief, Aircraft Laboratory
Directorate of Development

TABLE OF CONTENTS

LIST OF FIGURES

LIST OF FIGURES (Cont'd)

LIST OF SYMBOLS

a	blast wave shape parameter (see Eq. 1)
p	pressure
p_1	initial expansion chamber pressure
p_2	pressure immediately behind the flow-initiating shock
p_4	initial compression chamber pressure
Δp	overpressure at any point in the blast-type profile
Δp_s	overpressure (p_2-p_1) immediately behind the flow-initiating shock.
t	time, usually measured from the instant that S reaches any given observation station
Δt	time interval between arrival of S and arrival of R' at a given observation station
Δt_s	time interval for shock S to travel from shock detector No. 1 to shock detector No. 2 (see Fig. 4)
t_{o_p}	positive overpressure duration of the blast-type profile
C	so-called contact surface which in shock tube flow separates the gas initially in the expansion chamber from that initially in the compression chamber
F	foot of the initial rarefaction wave
R	head of the initial rarefaction wave
R'	head of the reflected rarefaction wave
S	the flow-initiating shock wave
S'	the reflected shock wave
U	velocity of the flow-initiating shock
X_c	effective length of the compression chamber

LIST OF SYMBOLS (Contd.)

$X_{C_{OPT}}$ value of X_C when R' overtakes S just as S reaches the test section

X_T distance from the diaphragm to the test section

SECTION I

INTRODUCTION

The accurate prediction of the response of a given type of lift-supporting structure of an aircraft to blast waves depends upon an accurate knowledge of the air forces developed on the lifting surface when subjected to blast. Simple theories to predict these blast-induced loads have been developed; however, their correctness has not yet been determined by experimental checks. Indirect evidence of correctness of these air force predictions has been obtained by measuring the responses of aircraft structures to blast and comparing these responses with those predicted using the theoretical air forces. Such a means of checking the validity of an air force theory is unsatisfactory because of the insensitive indication by structural response of the applied air forces. A direct and sensitive means of determining the air forces produced on a wing subjected to a blast wave is therefore required.

It is obviously inadvisable to rely exclusively on air force data from full scale field tests where blast waves are used, because of the difficulty of control to obtain the desired testing conditions, the expense, and lack of desirable repeatability of inputs in desired data-checking experiments.

In view of these and numerous other factors, the logical approach to a reliable experimental determination of the air forces produced on airfoils subjected to blast waves is considered to be through systematic laboratory testing supported by a limited number of full scale tests. In exchange for the advantages of laboratory testing, a sacrifice is made in that scale (blast wave duration and airfoil size) is not preserved. It is believed that in general this sacrifice of scale is of minor importance in this transient air force problem. The confirmation of this would be the objective of full scale tests.

Laboratory testing using explosive charges in an open area to produce blast waves for airfoil tests involves space and handling difficulties, and the problem of actually measuring the conditions at the surface since the airfoil is moving in respect to the observer. These problems are eliminated in the shock tube. What one does sacrifice in the latter case is the ability to let the blast approach at an arbitrary angle to the direction of initial flight, unless the cross section of the tube is very large.

Manuscript released by the authors April 12, 1956 for publication as a WADC Technical Report.

The term blast wave will be employed to describe the pressure wave emanating from an explosion in a three-dimensional space of uniform ambient conditions. This definition will be made more specific below. The term blast-type wave will be applied, where necessary for clarity, to waves that are generated by other means, such as in a shock tube, but have characteristics approaching those of a true blast wave.

There are five rather obvious means of generating blast-type waves in the conventional shock tube. These are:

(1) The use of explosive material (in a variety of arrangements)

(2) The shock tube is used in a conventional manner except that the primary shock which is generated is reflected from an elastically supported diaphragm of very small mass located just upstream of the test section of the tube. This results[1] in a shock wave followed by an overtaking rarefaction wave--a blast-type profile is thus observed at the test section.

(3) The expansion-chamber end of the shock tube is open to the atmosphere, so that after the shock wave reaches the end of the tube it expands in a radial fashion.[2]

(4) A partition is placed across the expansion chamber that has in it a slit extending from one wall to the other. Downstream from the slit is connected a two-dimensional diffusor so that the shock passing through the slit grows as a segment of a cylindrical blast-type wave.[3]

(5) The fifth method consists of adjusting the length of the compression chamber such that when the shock tube is operated in the conventional manner, the head of rarefaction wave which is reflected from the closed end of the compression chamber overtakes the primary shock just as it reaches the test section. A blast-type profile is thus formed.

Method (1) involves the disadvantages inherent in handling and storing explosives. Precise repeatability of test waves is also difficult to attain. Products of combustion lead to deposits on the shock tube walls and contamination of the testing medium. These latter problems, however, can be treated satisfactorily.

Method (2) offers ease of repeatability but attainable strengths and positive durations of the blast-type profiles generated appear to be limited (small range of short durations is obtainable), too limited to be practical for routine testing where a variety of blast-profile strengths (and possibly positive durations) are required.

Method (3) affords a fairly repeatable spacial peak-pressure decay, but the noise problem associated with an open-ended tube would make testing prohibitive in many laboratories for all but the very weak shock overpressures. It is also difficult to employ optical measurements, which are very useful for their good time and space resolution of flow field characteristics.

Method (4) appears to afford repeatable spatial pressure distributions, but the duration of the blast wave is too short for many experimental applications.

In Method (5), repeatability appears to be readily attainable. For routine testing purposes, this method is also well suited operationally. A variety of peak overpressures is readily obtainable by means of the conventional pressure-pressure technique of generating shock waves in the shock tube.

Since Method (5) appeared to be the most promising of the aforementioned methods for producing a blast-type profile in the shock tube for routine aerodynamic testing purposes, the measurements described herein were made to:

(a) make an evaluation of the facility and suitability of method (5) for routine testing purposes,

(b) obtain "calibration" data which could serve as reference information for future testing, and

(c) examine the shapes of the profiles thus obtained and to assess their general similarity to blast wave profiles.

It should be pointed out clearly at this time that the testing (critical assessment by means of experimental data) of aerodynamic theories to predict the lift-time history of airfoils subjected to blast waves does not in general depend upon obtaining experimental air force data on airfoils which are subjected to waves which duplicate precisely those of a blast profile in every detail. A flow which is similar in

character to that of a blast wave will generally suffice for a test flow field. If theoretical predictions of air forces produced on airfoils enveloped by "blast-type" shock tube profiles are verified by experiment, confidence would be established in such theoretical methods when applied to the condition of envelopment of an airfoil by a slightly different wave profile, the blast wave profile.

SECTION II

EXPERIMENTAL PROGRAM

2.1 Shock Tube Configuration

The shock tube used in these studies is described in reference 4. The pertinent dimensions are shown in Fig. 1. In brief, it consists of a tube having a uniform rectangular cross section of 8 by 24 inches throughout its 98-foot length. A Lumarith membrane (or diaphragm) is placed across the tube cross section dividing the tube into two chambers. In normal operation room air is pumped into the compression chamber until its pressure is a pre-selected amount larger than the pressure in the expansion chamber. When the pre-selected initial pressures have been produced in each chamber, the diaphragm which is highly loaded and stressed because of the pressure difference in the two chambers is punctured by a mechanically-operated knife. The high-pressure air is released into the expansion chamber; a shock wave forms and travels down the expansion chamber. Simultaneously a rarefaction wave advances into the high-pressure (compression) chamber, reducing the pressure in that chamber as it advances. These wave systems are depicted in Fig. 2.

When the compression chamber length X_C as shown in Fig. 2 is of the length shown compared to the distance X_T from the diaphragm to the test section, a step-function pressure profile is observed at the test section. However, if the compression chamber is shortened sufficiently compared to the length X_T, the head R' of the reflected rarefaction wave will overtake the flow-initiating shock, S, before the shock has reached the test station. A disturbance wave in the flow region generated by the shock S can always overtake the shock since the speed of the shock is subsonic with respect to conditions behind the shock. The speed of the shock is supersonic, however, with respect to conditions ahead of the shock.

Figure 3 illustrates the wave system in a shock tube whose compression chamber length is short enough that R' overtakes S just as S reaches the test section. This profile, it will turn out, best duplicates the blast profile, and gives the longest test period, therefore the corresponding value of X_C will be called $X_{C_{OPT}}$. Part (b) of Fig. 3, illustrates the type of

pressure profiles observed at the test station when $X_C > X_{C_{OPT}}$, when $X_C = X_{C_{OPT}}$, and when $X_C < X_{C_{OPT}}$. One objective of the present tests was that of determining $X_{C_{OPT}}$ for each of a series of initial pressure ratios p_4/p_1.

In this discussion, X_T has been implied as fixed. In the one-dimensional ideal shock tube only the ratio X_C/X_T is necessary to specify the wave system, until reflections from the end of the expansion chamber take place. But in the real shock tube due to the three-dimensional nature of the initial wave formation at the diaphragm section, and wall effects, it is necessary to specify both X_C and X_T. In all the present tests, X_T was fixed at 41.1 ft.

The compression-chamber length was varied by installing a "false end" within the existing compression-chamber cross section. The "false end" was constructed as shown in Fig. 4. It consisted of two 1/2" thick steel plates and four long 1 1/8" diameter screws. The first plate was the false-end plate fitted neatly inside the compression chamber and acting as the compression-chamber end. It was mounted and supported longitudinally by the four long screws threaded through the actual end plate of the shock tube. Due to the length of the screws, a second steel plate was placed midway between the false end plate and the actual end plate to insure the screws from buckling under high compression chamber pressure. With such an arrangement the effective length could be varied from 22 1/4" to 48" (or more) with ease by advancing or retracting the four screws.

2.2 Instrumentation

A block diagram of the pressure-measuring system is shown in Fig. 5.

The pressure transducer employed is a 0-100 p.s.i. Dynasco gage with a diaphragm and a four-arm strain-gage sensing element (made by Dynamic Inst. Co.). It was placed 41.1 ft. from the diaphragm section and mounted flush with the shock tube wall during all experiments. It has a linearity within 0.5 per cent over the whole range, a sensitivity of .32 millivolt per psi with a ten volt excitation. The overall resistance is 600 ohms. The natural frequency was found to be approximately 14 kilocycles. The diameter of the transducer is 9/16".

A Furst wide-band D.C. amplifier was used with a maximum gain of 100. The frequency response was found to be flat from

D.C. to 200 KC. The noise level of the amplifier was specified by manufacturer to be approximately 40 microvolts or less referred to the input.

Due to a low damping ratio of the pressure transducer (approximately 0.05), a small shunt capacitor (0.4 μfd) was used between the amplifier and the oscillosynchroscope to filter out the excess amplitude at transducer resonance without too much sacrifice of the overall frequency response. The actual frequency response of the amplifier-filter unit was determined experimentally and, together with the transducer performance obtained previously, the frequency response of the complete pressure measuring system was computed and plotted in Fig. 6. The rise time of the complete pressure sensing system was found to be 0.2 milliseconds.

The signal was displayed on a Browning oscillosynchroscope model OA-16 and recorded by a manually-synchronized Dumont oscillograph record camera. The oscillosynchroscope has a bandwidth of D.C. to 5 megacycles and a horizontal sweep rate ranging from 2 microsecond to 1 sec per centimeter. The sweep linearity was found to be within 5 per cent over the whole screen. The horizontal time scale was calibrated before each run by using a square-wave generator.

The horizontal sweep of the oscillosynchroscope was triggered by the signal generated in Schlieren System No. 1 located 70" upstream from the pressure transducer. The passage of the shock by the Schlieren detector deflected the narrow light beam about the knife edge of the schlieren pick-up, which (light beam deflection) was detected by the photo-multiplier tube and caused a sharp voltage pulse to appear at the output of the Schlieren Detector. The output of Schlieren System No. 1 was then fed into a cascade of an electronic gate amplifier and a variable time-delay generator which in turn triggered the oscillosynchroscope. The amount of time delay was pre-set according to the shock speed expected, such that the sweep of the oscillosynchroscope was triggered shortly before the shock arrived at the pressure transducer. The exact amount of time delay for each test was registered in counter B which was in parallel with the time-delay generator.

For the purpose of determining the shock speed, another Schlieren System (No. 2) installed at exactly 3 feet downstream from Schlieren System No. 1 was used together with Schlieren System No. 1 and a 1/1,600,000-second-increment Potter counter chronograph. The time interval between the pulse signals generated by the two schlieren systems as the shock passed, Δt_s, was measured and thus the shock speed was determined. This measurement is believed to be accurate to within 0.2 per cent.

2.3 Test Procedure

Tests were conducted for a series of initial pressure ratios p_4/p_1 (ranging from 2 to 21) for each of a series of effective compression chamber lengths X_C (ranging from 22 1/4 to 48"). In all cases, the diaphragm to test section distance was 41.1 feet.

Before each run, the temperature of the ambient atmosphere was observed and was assumed to be the temperature of the air in the expansion chamber before firing. Check measurements show this assumption generally to be acceptable. The shock velocity U was measured, as described earlier, during each test run.

During each run, the pressure profile occurring at the test section was recorded by using an appropriate sweep rate on the oscillosynchroscope tube for the time base; the ordinate represented the observed pressure. The resulting trace was photographed. For each combination of compression chamber length X_C and initial pressure ratio p_4/p_1, two sweep rates were used: (a) four milliseconds for full horizontal scale and (b) twenty-five milliseconds for full horizontal scale. The four millisecond sweep rate was used to define critically the time elapsed between shock arrival and arrival of the head R' of the reflected rarefaction wave. The twenty-five millisecond sweep rate was used to record the general shape of the pressure profile.

Effective compression chamber lengths X_C of 22 1/4, 32, 40, and 48 inches were used at initial pressure ratios p_4/p_1 of 2, 2.8, 3.7, 5.0, 6.2, 8.5, 9.5, 10, 12.4, and 21.6. After the initial pressure p_1 was set for each run, firing was delayed approximately one minute to permit the temperature to settle to the room temperature value. The measured pressure-time curves are shown in Fig. 7a to 7s. For reasons to be explained later, the scale of each oscillogram was adjusted so that the distance on the coordinate between the pressure peak and the half-way fall-off point was the same.

SECTION III

RESULTS

3.1 Determination of $X_{C_{OPT}}$.

Figure 8 illustrates a typical pressure profile for $X_C > X_{C_{OPT}}$, which will be used to describe the results obtained. The solid curve represents the actual pressure at the test station, whereas the dashed line corresponds to the measured value due to the time lag of the transducer. The uncertainty in the determination of $X_{C_{OPT}}$ is primarily due to this time lag; therefore, the method used to arrive at $X_{C_{OPT}}$ will be carefully described.

(1) The initial rise point of the measured pressure in the test oscillograms can be determined quite accurately. For sufficiently large values of Δt the existence of a small noise and resonance signal causes an uncertainty in determining the arrival of the head of the rarefaction wave by approximately 0.4 milliseconds. The data, therefore, had to be extrapolated to find the value of X_C corresponding to $\Delta t = 0$. The Δt data are shown in Figs. 9a to 9j. In view of the uncertainty connected with the extrapolation, additional information was believed advisable.

(2) The peak value of the overpressure, Δp_{max}, was measured from the test oscillograms as shown in Fig. 9a to 9j. As the compression chamber is shortened, the actual value of Δp_s would be constant until X_C becomes less than $X_{C_{OPT}}$. Actually the oscillograph data would begin to fall off at a somewhat greater value of X_C due to the time lag of the transducer. These data might appear to be a more reliable means of determining X_C than method (1) since the latter requires that the pressure curve develop a definite flat portion to clearly identify the arrival of the rarefaction wave. Actually, the uncertainty in determining Δp_s from the oscillograms, approximately 3 per cent, combined with the scatter in Δp_s between runs with the same initial pressures, makes the uncertainty of method (2) essentially equal to that of method (1). The two methods thus afford supplementary data.

(3) As the length of the compression chamber is shortened still further, the reflected rarefaction wave overtakes the shock ahead of the test station; and, if X_C is sufficiently reduced, the shock is overtaken ahead of Schlieren System No. 2. When this occurs, the shock speed between the two Schlieren systems is reduced and the time interval, Δt_s, between the two systems is increased. The Δt_s data are also shown in Figs. 9a through 9j. The second Schlieren system is 34" upstream from the test station (see Fig. 1); so for $X_T/X_{C_{OPT}} = 17$, a typical value for these tests, Δt_s would deviate from a constant value when the compression chamber was shortened to $X_C = X_{C_{OPT}} - 2$ inches. The Δt_s data are not sufficiently reliable to determine this value of X_C, but they can be used to set a lower limit in arriving at $X_{C_{OPT}}$. In reality it is satisfactory if the reflected rarefaction overtakes the shock anywhere between the second Schlieren system and the test station as the effect on the blast-type profile is negligible.

The values of $X_{C_{OPT}}/X_T$ obtained from the data shown in Figs. 9a through 9j are given in Fig. 10 as a function of initial pressure ratio p_4/p_1. The theoretically-predicted curve of $X_T/X_{C_{OPT}}$ given in reference 5 is shown in Fig. 10 for comparison. Uncertainty brackets are shown for the experimental data.

3.2 Characteristics of the Blast-Type Profiles

When $X_C = X_{C_{OPT}}$, the overpressure profile produced is seen to be similar in shape to the blast profile produced by a free-air explosion. Such a blast overpressure profile can be approximated analytically by the following expression[6]:

$$\Delta p = \Delta p_s \left(1 - \frac{t}{t_{o_p}}\right) e^{-a \frac{t}{t_{o_p}}} \qquad (1)$$

where

Δ_p is the overpressure at any point in the blast wave profile

Δp_s is the overpressure immediately behind the shock front heading the blast wave

t is time measured from the instant that the blast wave shock front arrives at the subject observation station

t_{o_p} is the (time) duration of the positive phase of blast-wave overpressure

a may be considered as the blast-wave shape parameter.

For an explosion occurring in a homogeneous atmosphere of infinite extent, "a" is found to be a function of $\Delta p_s/p_1$, where p_1 is the pressure of the ambient atmosphere through which the shock is propagating. The profile given by the above equation is shown in Fig. 11.

For many shock tube testing purposes (aerodynamic measurements and elastic model response studies, for example), it is important that the shape of the "blast-type" profile produced in the shock tube be similar to that of a true blast wave only during the positive overpressure phase of the blast wave.

A useful qualitative comparison of shapes is obtained by using the above analytical relation for overpressure, taking "a" as 0.5 as is the case for weak blast waves, and comparing the resulting shape with the decaying portion of the overpressure profiles shown in Figs. 7a through 7s. This comparison was carried out by constructing five templates representing Eq. 1 with Δp_s corresponding to 1, 1.5, 2, 2.5, and 3 inches, but with a time scale identical to that of the oscillograms. Recall, Div. 2.3, that all of the oscillograms had been enlarged so that the time coordinate between the pressure peak and the half-way fall-off point was equal. For each oscillogram one or two of these templates were chosen to match or compare in shape with the observed pressure profile. These comparisons are shown in Figs. 7a through 7s by the dashed lines.

Since the observed profiles had no negative phase, the analytical representation cannot be expected to compare exactly near the end of the positive phase of the observed profiles. This is expected due to the one- and three-dimensional nature

of the two cases. They are in good agreement until the overpressure falls to about 15 to 40 per cent of Δp_s. The approximation appears to be better where the shock-wave rarefaction-wave interaction began at the test section, and also at the lower values of p_4/p_1. The shock tube profiles exhibit a less rapid decay near the end of the positive phase than do blast waves.

It is not a matter of great concern to note that the pressure profiles produced in this series of experiments are not precisely blast-like at later times, because in general the pressure step at the shock and the initial rapid pressure fall-off will be the most critical portion of the wave insofar as the air forces on an (elastic) wing and the dynamic response of such an airfoil to this airloading is concerned. A precise determination of the duration, t_{o_p}, of the positive overpressure phase of the shock tube profiles is not afforded by these profiles; hence a more detailed examination of the profile shapes and their dependence upon p_4/p_1 is not presented.

Examination shows that for each initial pressure ratio, the time required for the pressure to decay to one-half of the pressure immediately prior to the arrival of R' increases as X_C increases. This is, of course, to be expected since rarefaction waves tend to become less steep as they propagate.

Figure 12 shows an experimental comparison (from reference 4) of p_4/p_1 vs $\Delta p_s/p_1$ with the ideal theoretical variation. This figure enables the shock tube operator to select the initial pressure ratio required to generate a shock wave of given overpressure, Δp_s, when p_1 has been specified.

SECTION IV

CONCLUSIONS

The reflection method has been found to be a feasible method of producing blast-type pressure profiles in the shock tube for routine testing purposes. Shock-tube profiles produced in this manner are seen to be strikingly similar to true blast wave profiles during approximately the first half (in some cases) and the first three-quarters (in other instances) of the positive phase; however, the pressure decay is less rapid than for a true blast wave during the remainder of the positive phase. The blast-type profiles which can readily be generated in the MIT tube in its present configuration, using air as the testing medium, decay in overpressure to ten per cent of the peak overpressure in times ranging from approximately 13 to more than 30 milliseconds, with shock overpressures ranging up to approximately 100 psi.

While these pressure profiles have been measured (and can in the future be measured more accurately now that better instrumentation is available), determinations of density and material velocity time histories are needed to define the flow adequately. It is believed that, for most practical purposes, analytical determination of profile density and material velocity would be adequate in view of the essentially isentropic character of the free-stream flow; direct experimental checks are desirable, however.

REFERENCES

1. White, D.R. and Weimer, D.K., A Method for Modification of the Pressure Profile in a Shock Tube, Technical Report II-12, Dept. of Physics, Princeton University, ONR Contract NR061-020, N6 ori-105, TASK II, April 1952.

2. Grady, L.P. and Beichler, G.P., Preliminary Investigation of the Shock Wave Propagated from the Open End of a Cylindrical Shock Tube, Ballistic Research Laboratories, Aberdeen Proving Ground, BRL Technical Note No. 843 (AFSWP No. 768), January 1954.

3. Peterson, E.H., Investigation of a Method for Generating a Cylindrical Shock Wave, Master of Science Thesis, MIT, Dept. of Aero. Eng., January 1956.

4. Witmer, Emmett A., Ruetenik, J. Ray, Beals, Vaughn L. Jr., Herrmann, Walter, The Design, Construction, and Operation of the MIT-WADC Shock Tube Facility, WADC TR 53-228 (in preparation).

5. Glass, I.I., Martin, W., and Patterson, S.N., A Theoretical and Experimental Study of the Shock Tube, University of Toronto, Institute of Aerophysics, UTIA Report No. 2, November 1953.

6. Cole, R.H., Underwater Explosions, Princeton University Press, 1948.

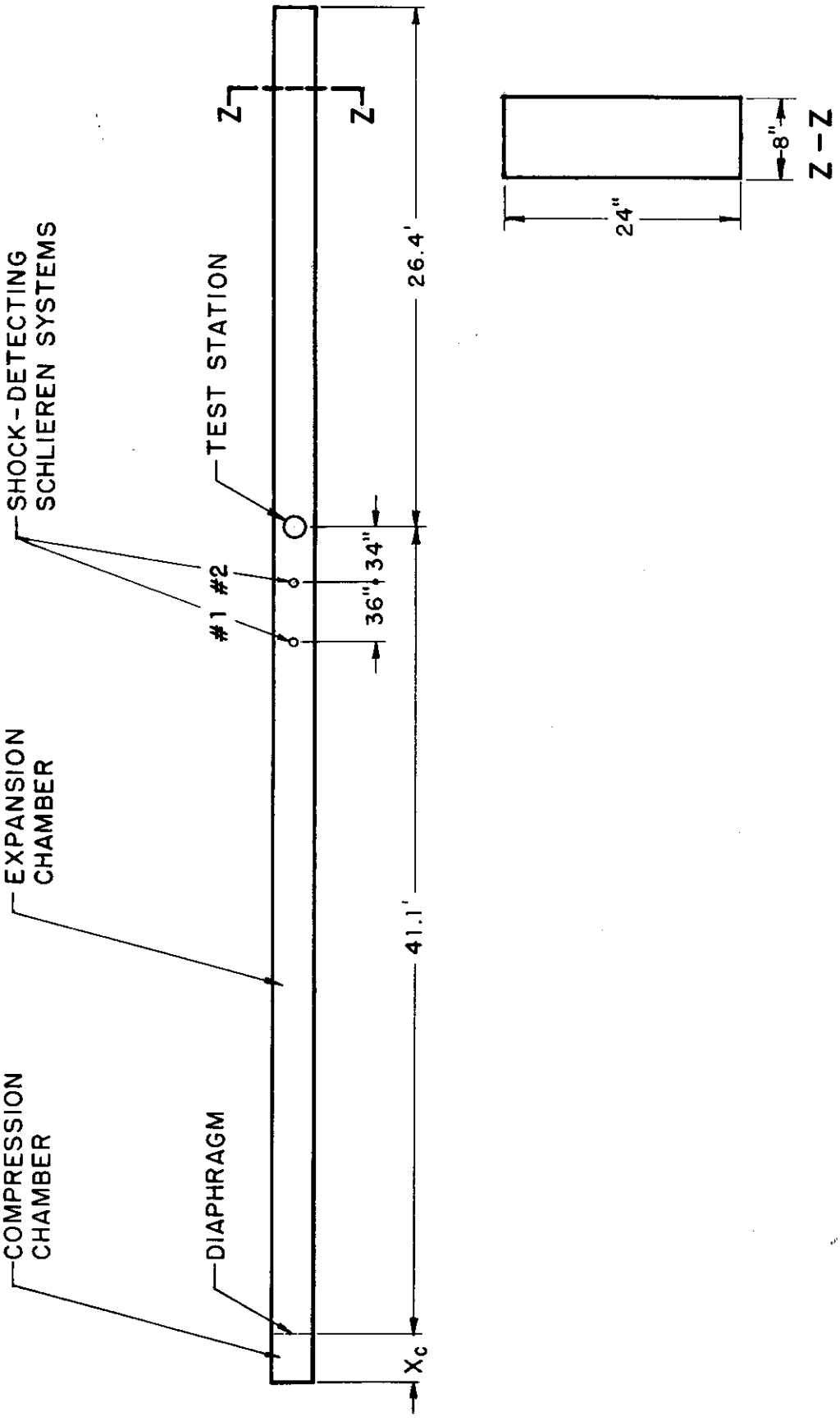

FIG. 1 PERTINENT DIMENSIONS OF THE SHOCK TUBE

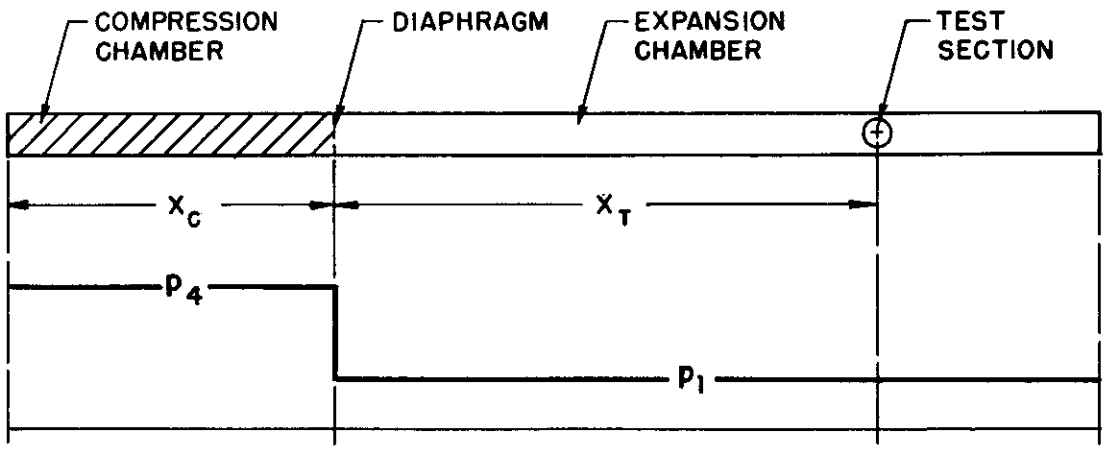

(a) PRESSURE DISTRIBUTION IN THE TUBE BEFORE DIAPHRAGM IS PUNCTURED

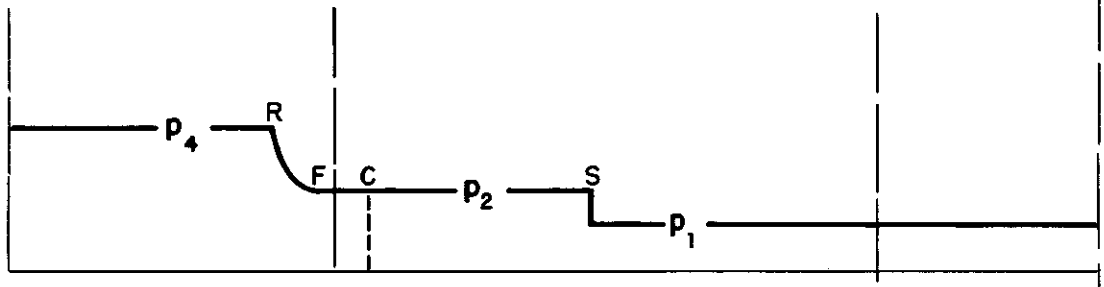

(b) PRESSURE DISTRIBUTION IN THE TUBE SHORTLY AFTER DIAPHRAGM BURST

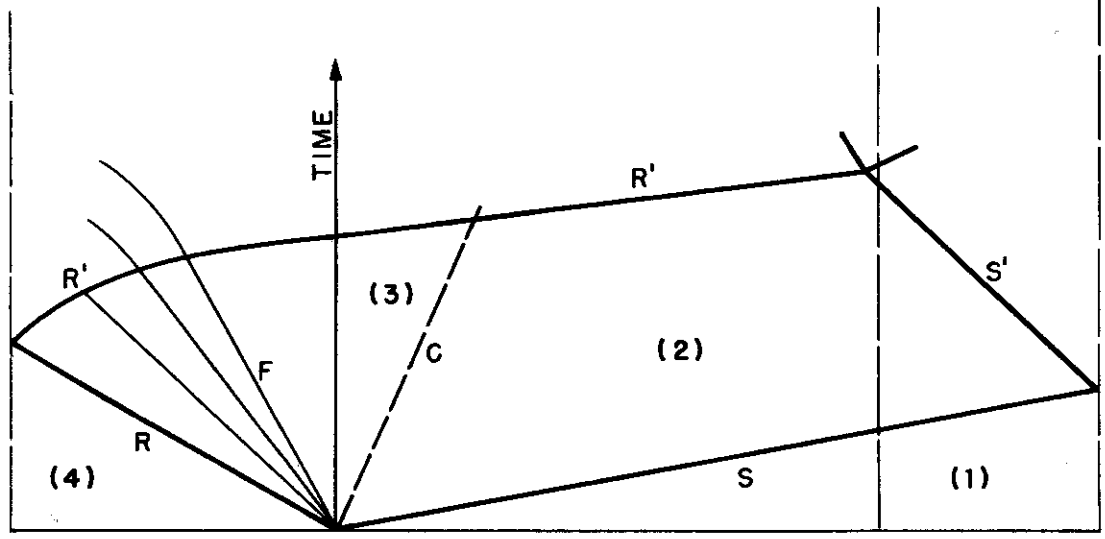

(c) DISTANCE-TIME DISPLAY OF WAVES IN THE SHOCK TUBE

FIG. 2 THEORETICAL WAVE SYSTEM IN A CONVENTIONAL SHOCK TUBE

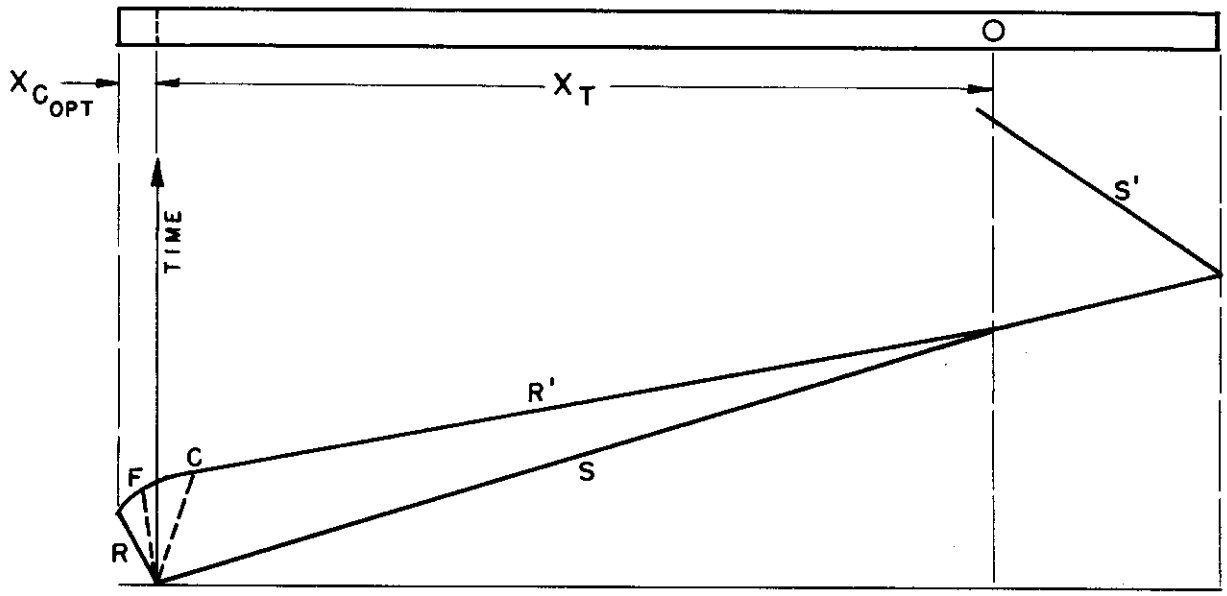

(a) WAVE-FRONT POSITION VS TIME WHEN $X_C = X_{C_{OPT}}$

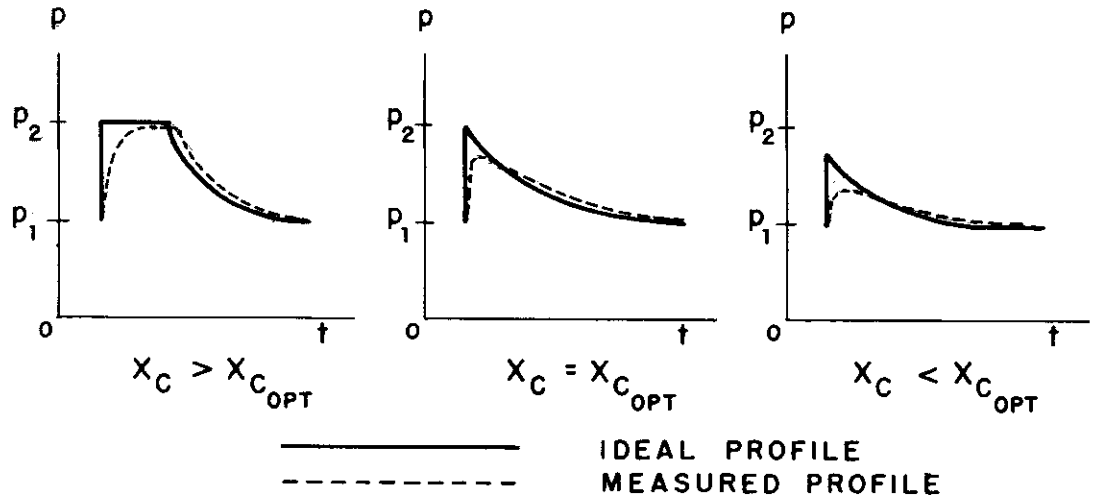

(b) PRESSURE – TIME PROFILES OBSERVED AT THE TEST SECTION FOR A GIVEN INITIAL PRESSURE RATIO, p_4/p_1

FIG.3 ILLUSTRATION OF WAVES AND PRESSURE PROFILES ASSOCIATED WITH BLAST-TYPE PROFILE PRODUCTION IN THE SHOCK TUBE

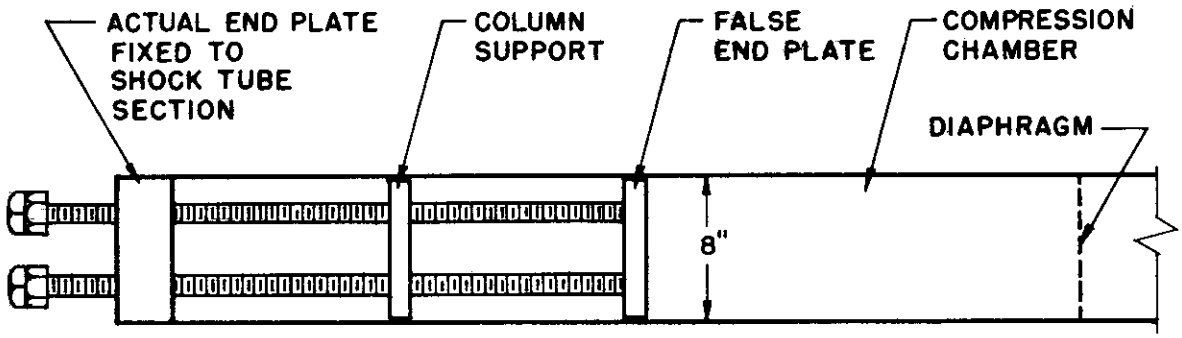

TOP VIEW

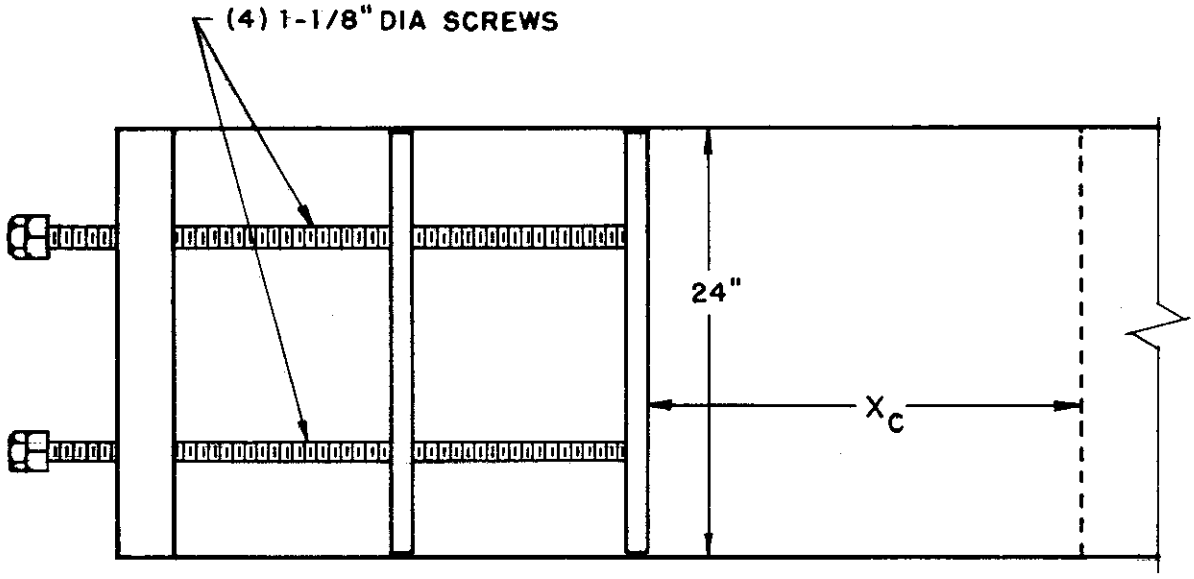

SIDE VIEW

FIG. 4 CONFIGURATION OF THE REFLECTION PLATE AND ITS SUPPORT

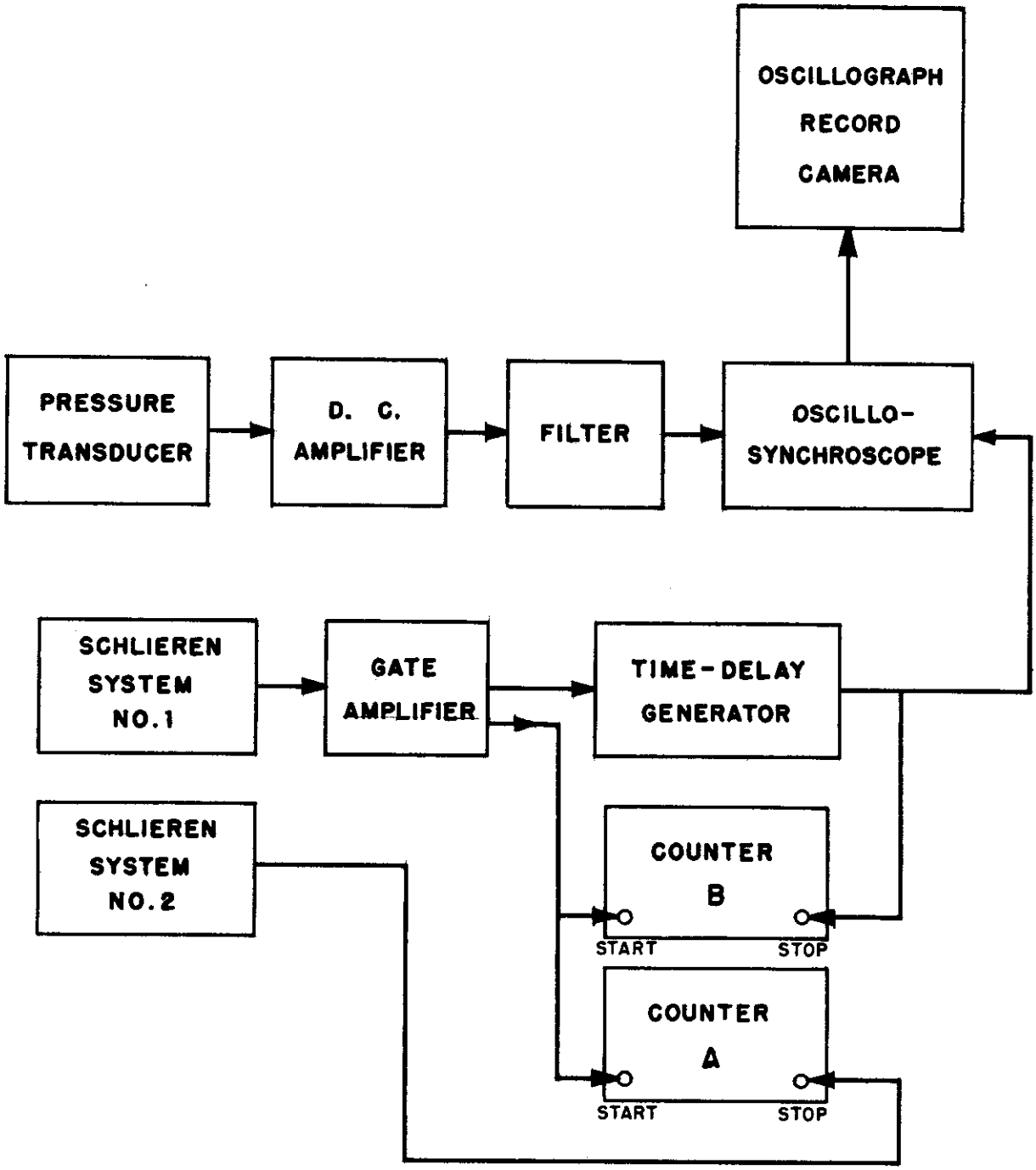

FIG. 5 BLOCK DIAGRAM OF THE INSTRUMENTATION

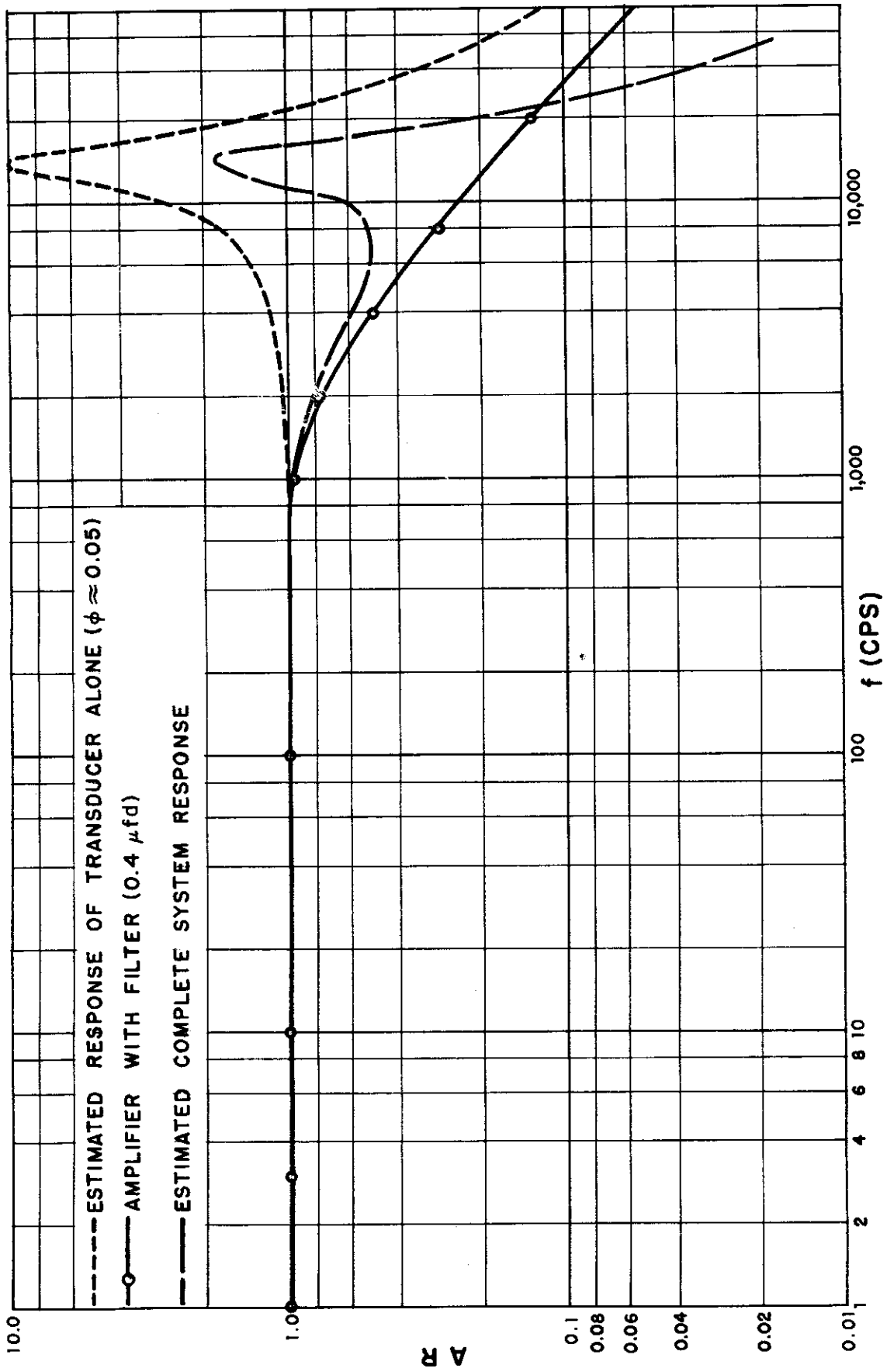

FIG. 6 FREQUENCY RESPONSE OF THE PRESSURE MEASURING SYSTEM

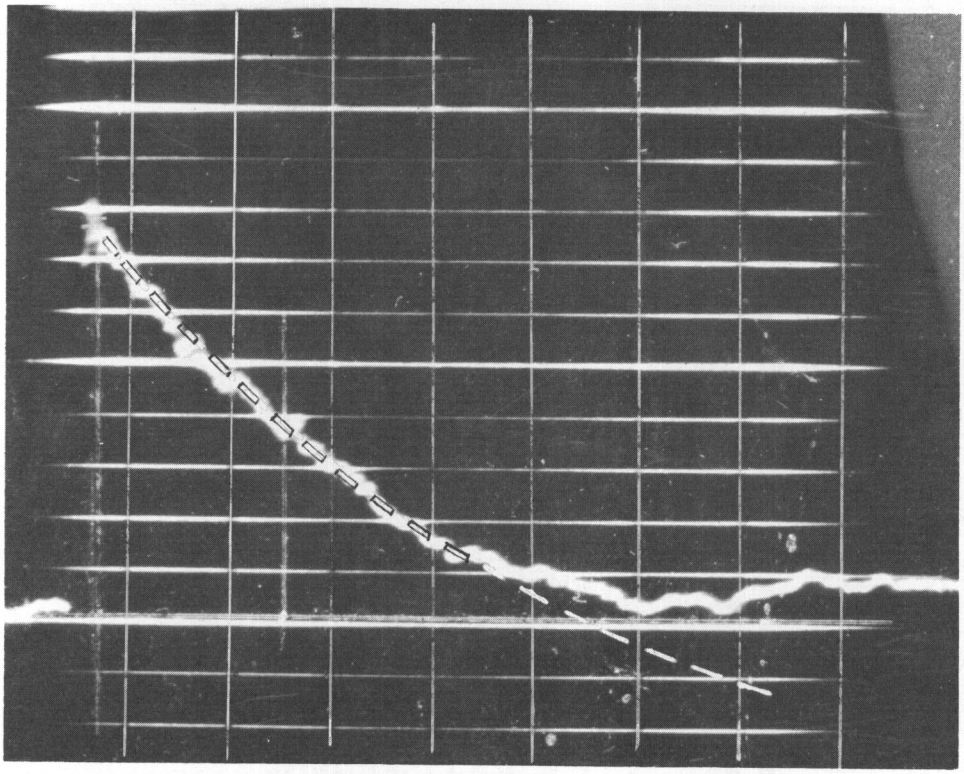

$X_c = 22\frac{1}{4}$"

HORIZONTAL SCALE = 2.5 MILLISECONDS / DIVISION
VERTICAL SCALE = 1 P.S.I. / DIVISION

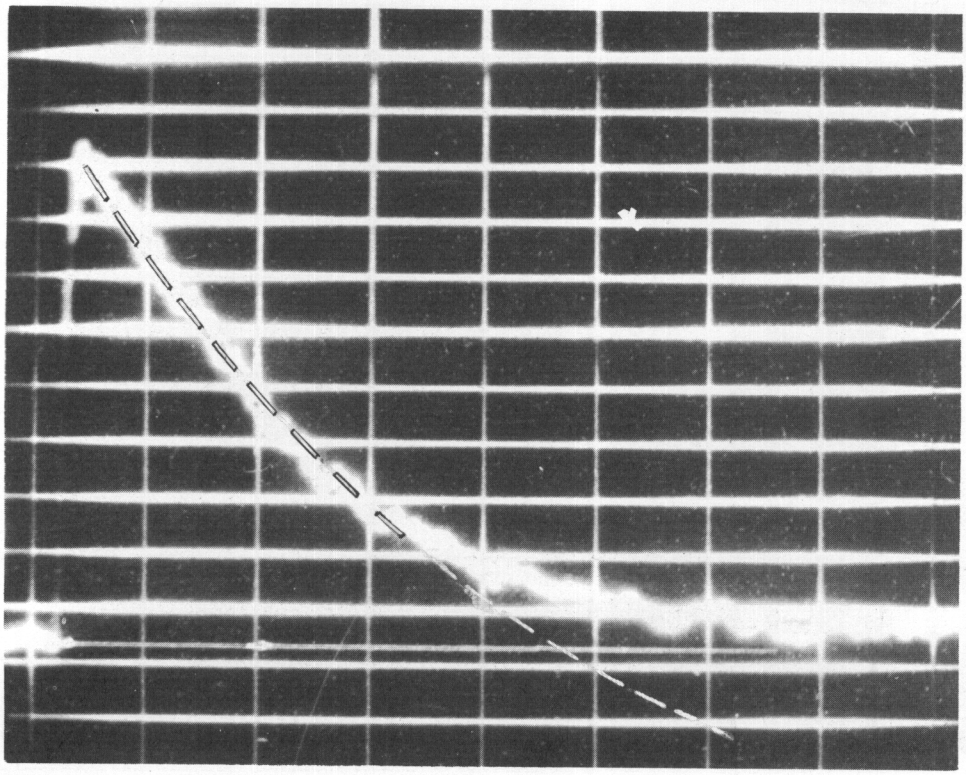

$X_c = 32$"

FIG. 7a MEASURED PRESSURE PROFILES, $p_4 / p_1 = 2.0$

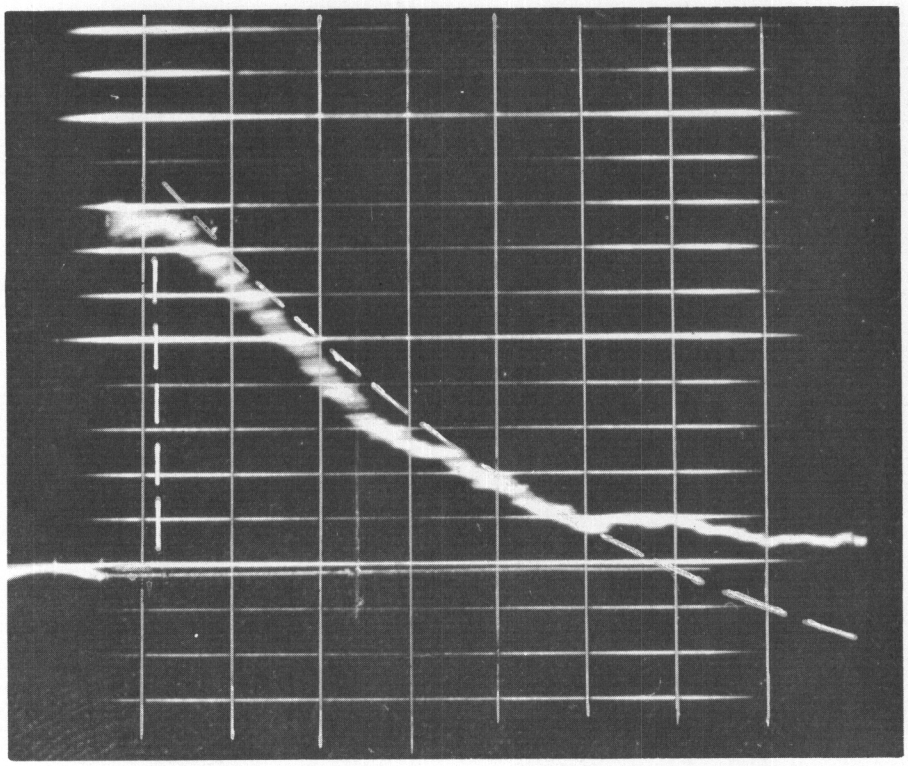

$X_c = 40"$

HORIZONTAL SCALE = 2.5 MILLISECONDS / DIVISION
VERTICAL SCALE = 1 P.S.I. / DIVISION

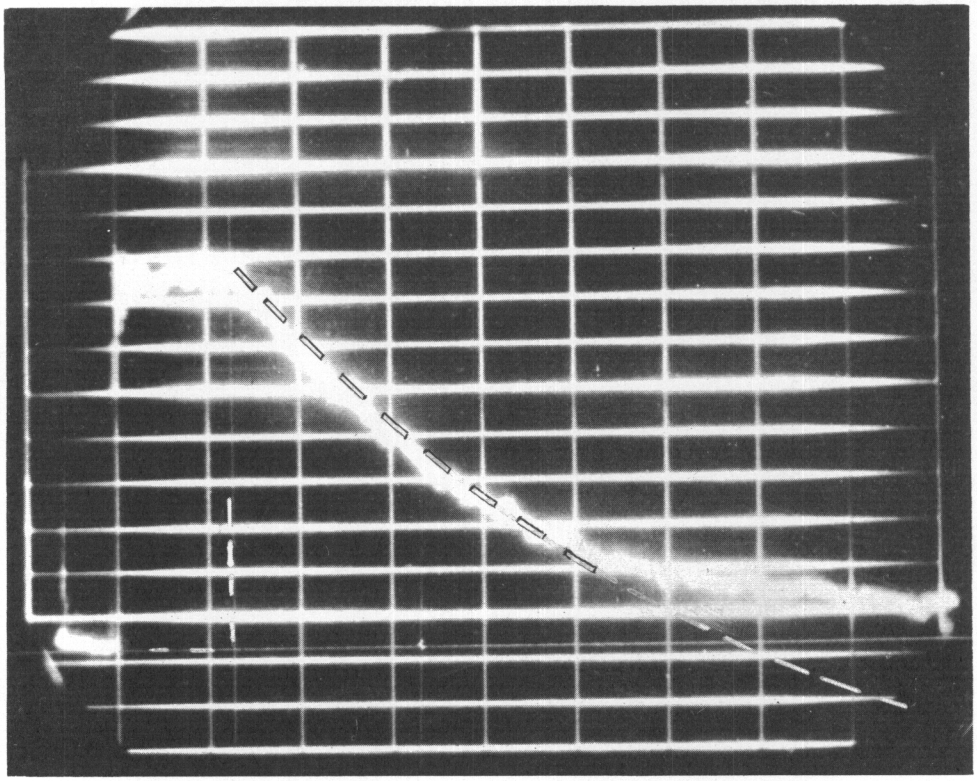

$X = 48"$

FIG. 7b MEASURED PRESSURE PROFILES, $p_4/p_1 = 2.0$

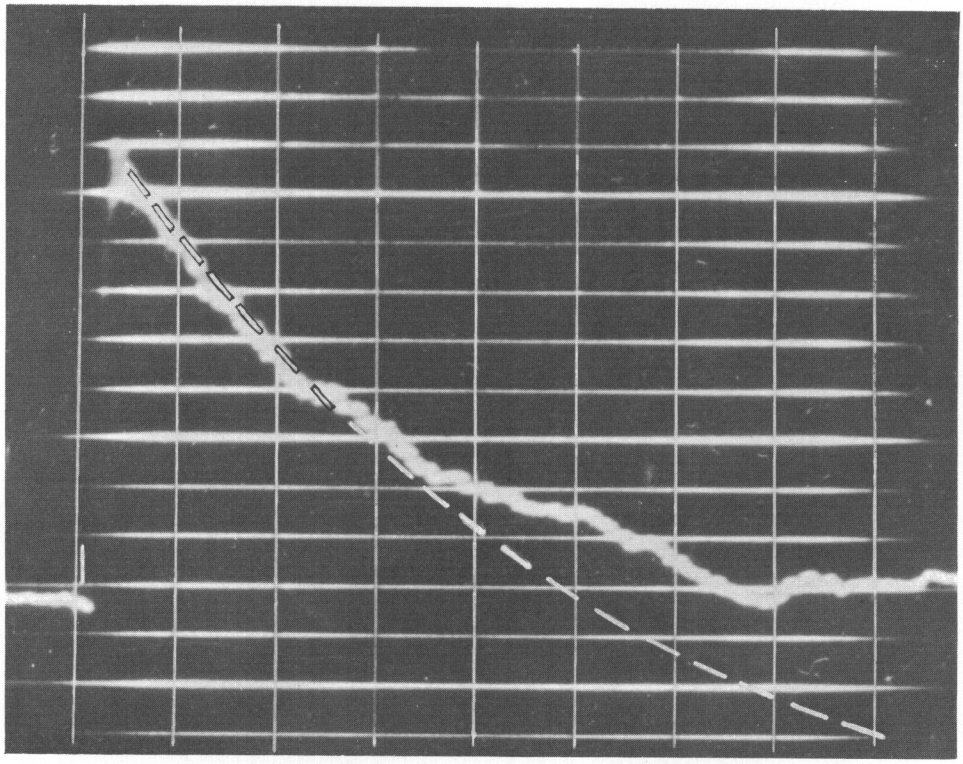

$X_c = 22\frac{1}{4}$"

HORIZONTAL SCALE = 2.5 MILLISECONDS / DIVISION
VERTICAL SCALE = 1 P.S.I. / DIVISION

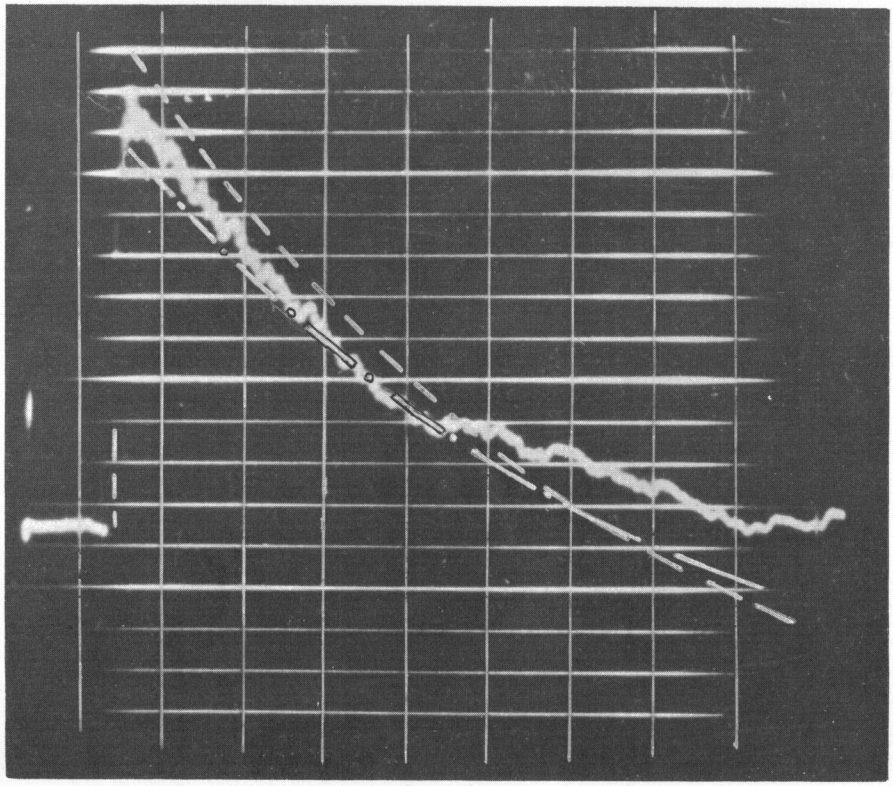

$X_c = 32$"

FIG. 7c MEASURED PRESSURE PROFILES, $p_4 / p_1 = 2.8$

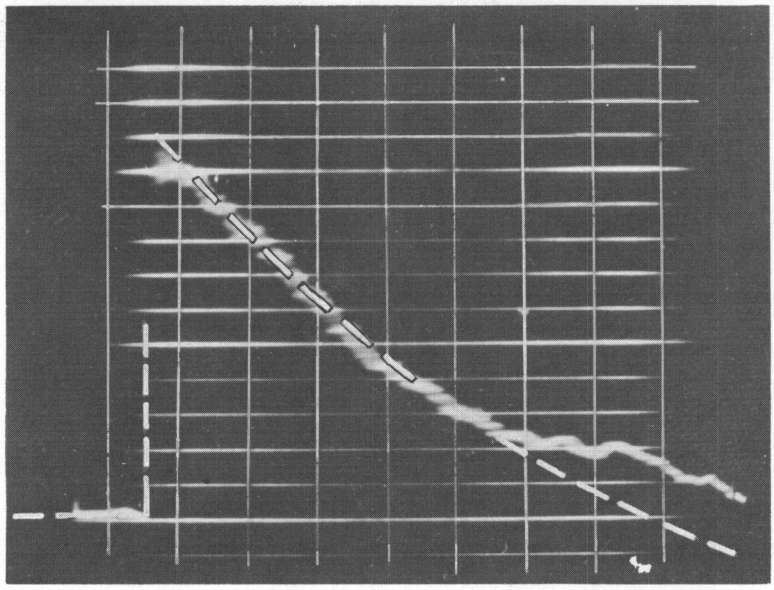

$X_c = 40"$

HORIZONTAL SCALE = 2.5 MILLISECONDS / DIVISION
VERTICAL SCALE = 1 P.S.I. / DIVISION

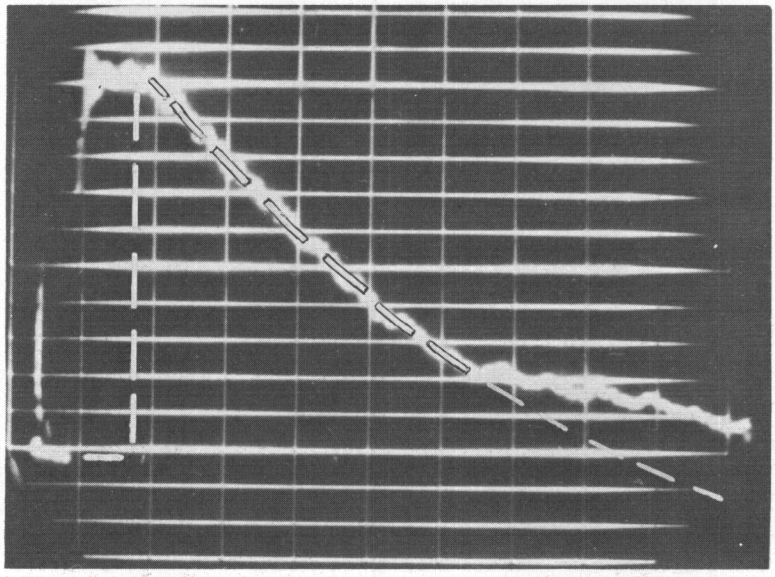

$X_c = 48"$

FIG. 7d MEASURED PRESSURE PROFILES, $p_4/p_1 = 2.8$

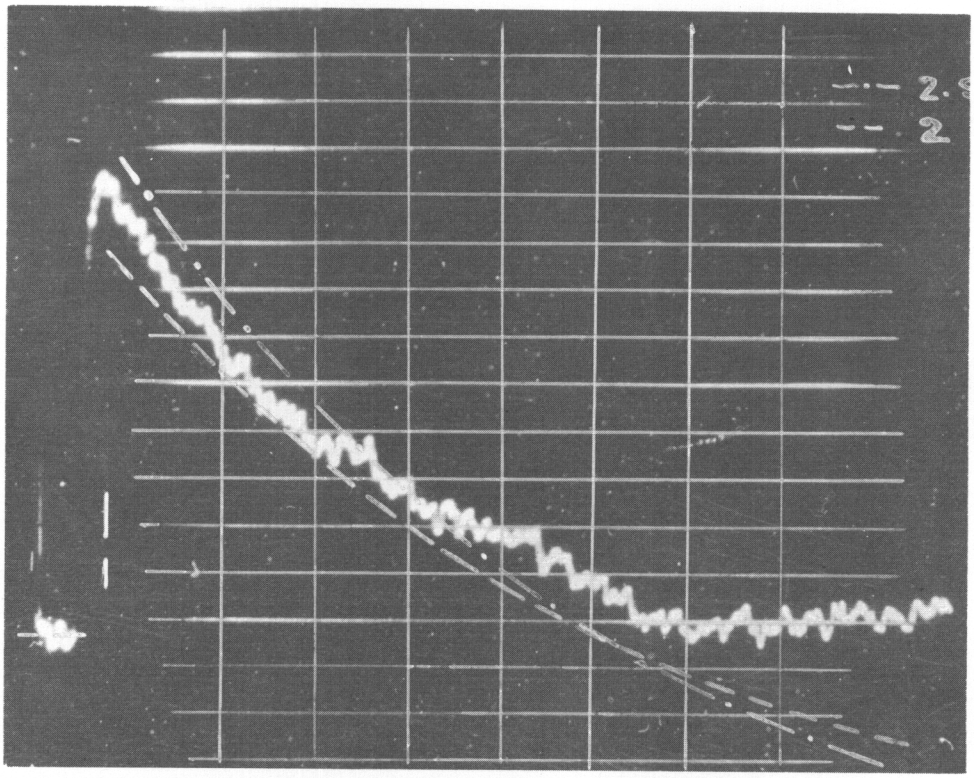

$X_c = 22\frac{1}{4}"$

HORIZONTAL SCALE = 2.5 MILLISECONDS / DIVISION
VERTICAL SCALE = 1 P.S.I. / DIVISION

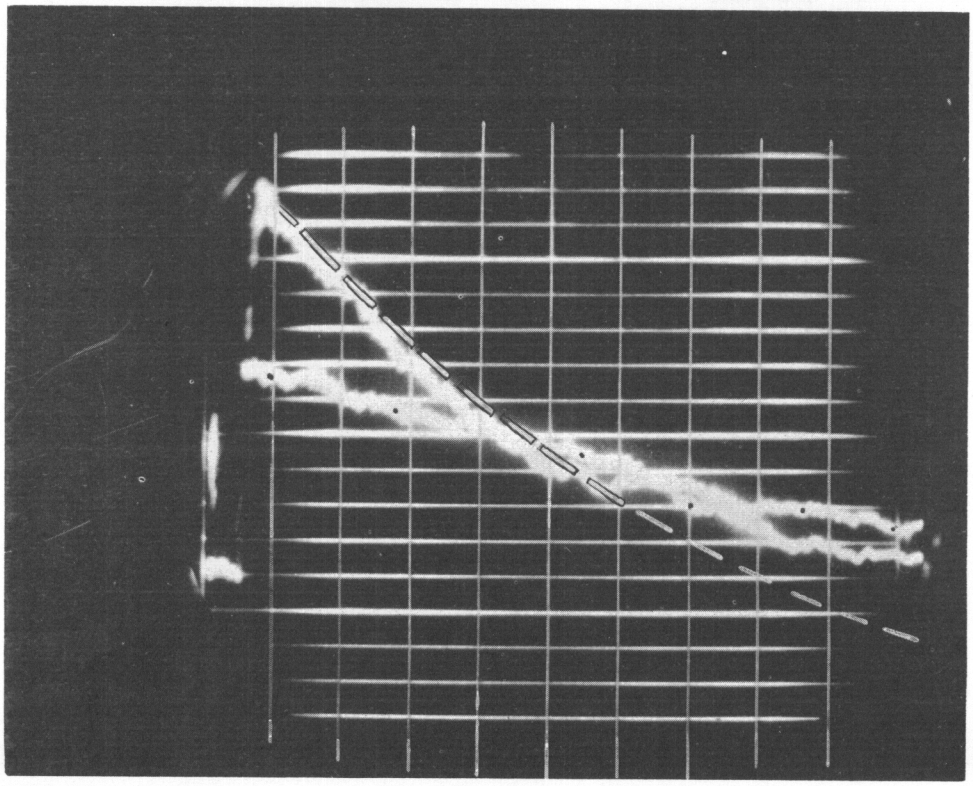

$X_c = 32"$

FIG. 7e MEASURED PRESSURE PROFILES, $p_4/p_1 = 3.7$

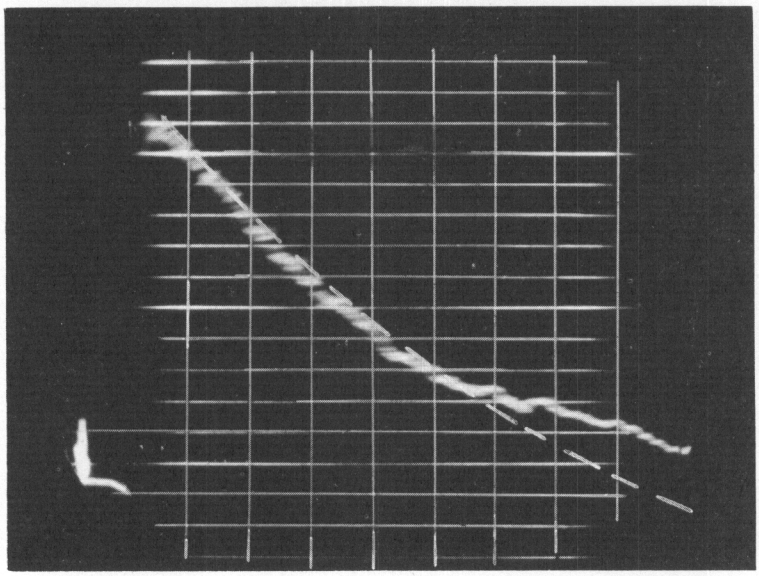

$X = 40"$

HORIZONTAL SCALE = 2.5 MILLISECONDS / DIVISION
VERTICAL SCALE = 1 P.S.I. / DIVISION

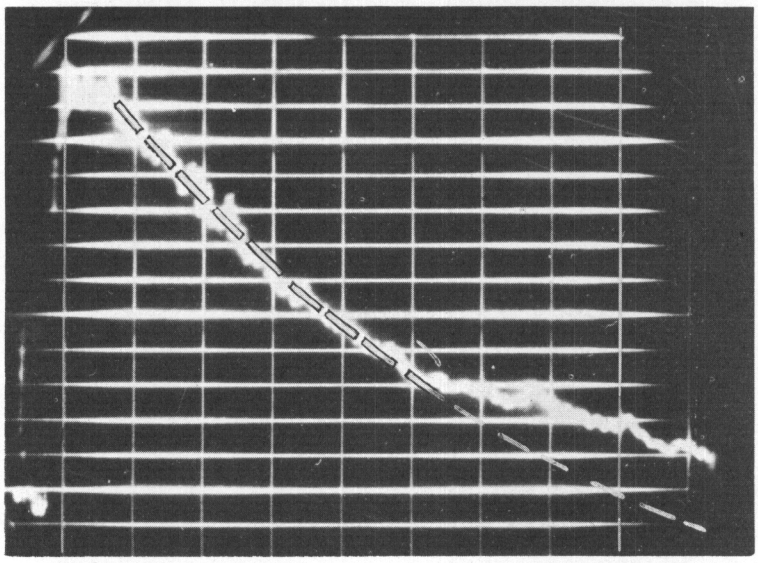

$X_c = 48"$

FIG. 7f MEASURED PRESSURE PROFILES, $p_4 / p_1 = 3.7$

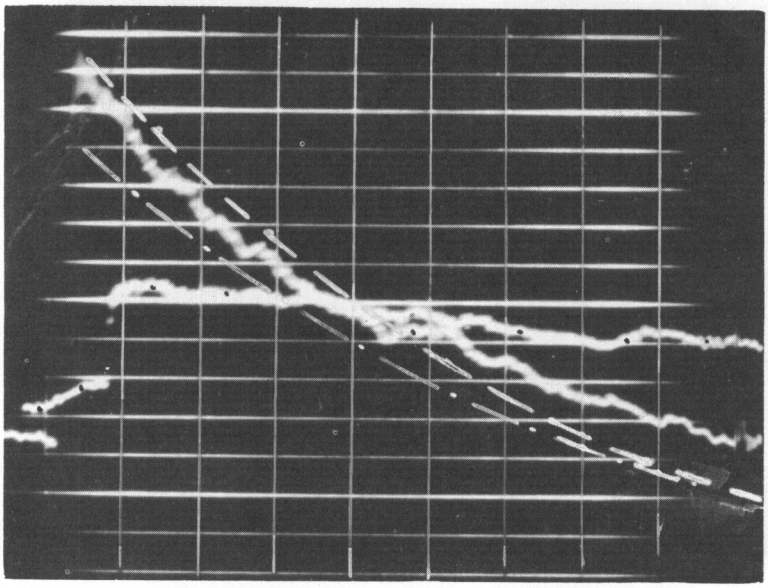

$X_c = 22\frac{1}{4}$"

HORIZONTAL SCALE = 2.5 MILLISECONDS / DIVISION
VERTICAL SCALE = 1 P. S. I. / DIVISION

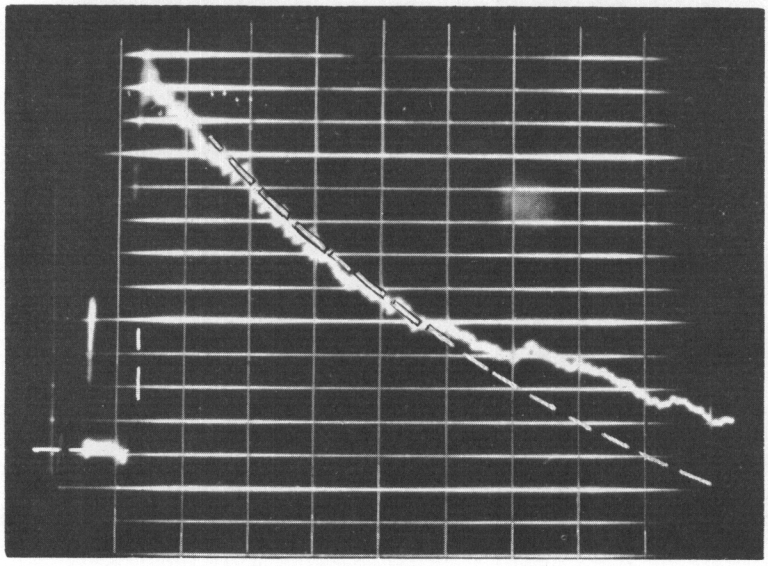

$X_c = 32$"

FIG. 7g MEASURED PRESSURE PROFILES, $p_4 / p_1 = 5.0$

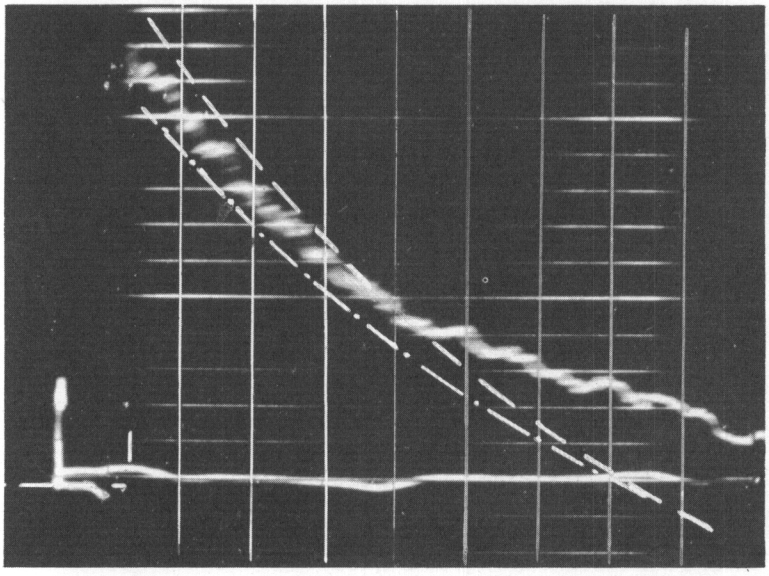

$X_c = 40"$

HORIZONTAL SCALE = 2.5 MILLISECONDS / DIVISION
VERTICAL SCALE = 1 P.S.I. / DIVISION

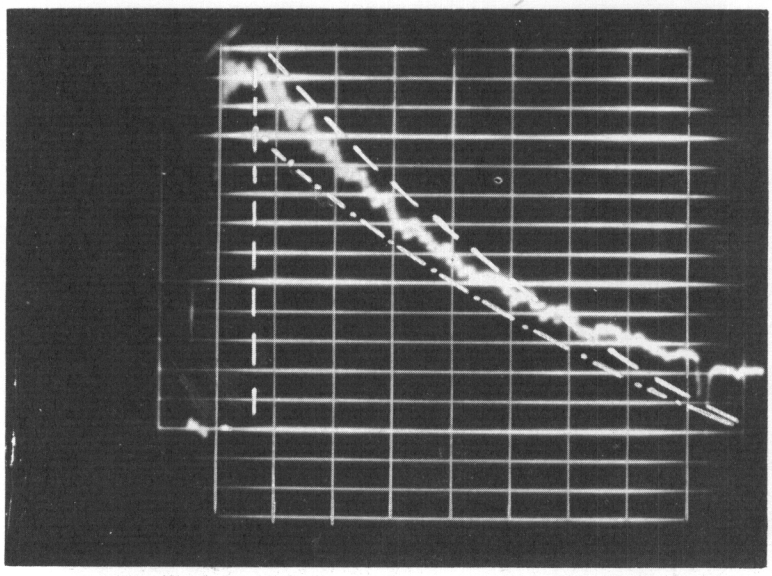

$X_c = 48"$

FIG. 7h MEASURED PRESSURE PROFILES , $p_4 / p_1 = 5.0$

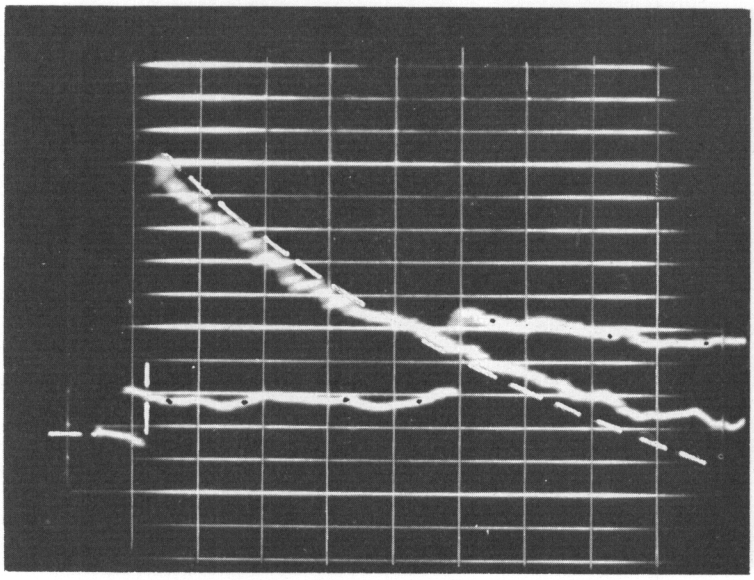

$X_c = 22\frac{1}{4}$"

HORIZONTAL SCALE = 2.5 MILLISECONDS / DIVISION
VERTICAL SCALE = 1 P.S.I. / DIVISION

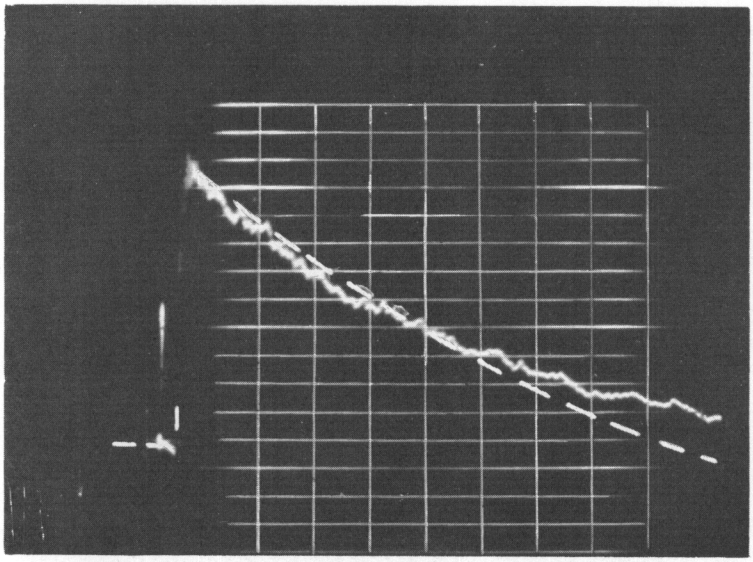

$X_c = 32$"

FIG. 7i MEASURED PRESSURE PROFILES, $p_4/p_1 = 6.2$

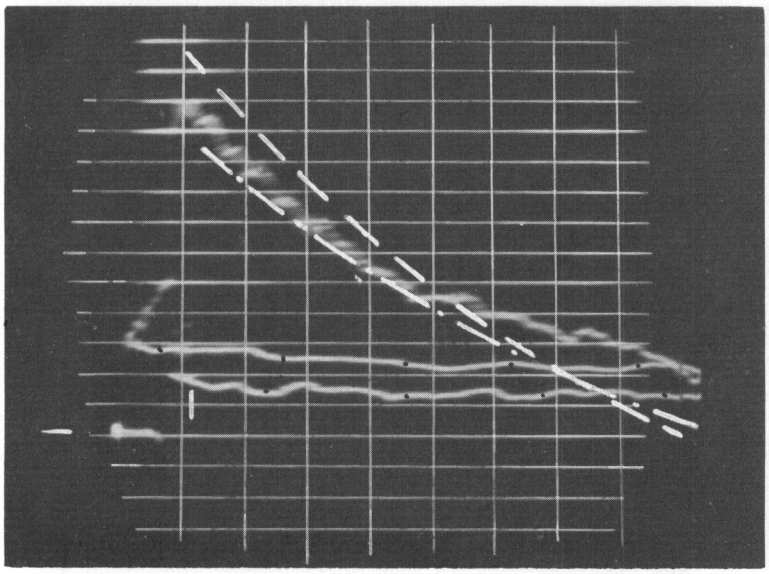

$X_c = 40"$

HORIZONTAL SCALE = 2.5 MILLISECONDS / DIVISION
VERTICAL SCALE = 1 P.S.I. / DIVISION

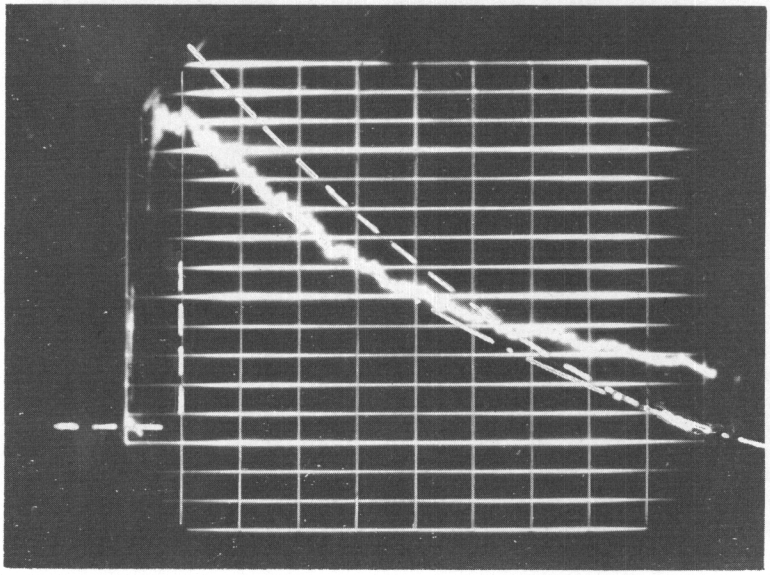

$X_c = 48"$

FIG. 7j MEASURED PRESSURE PROFILES, $p_4 / p_1 = 6.2$

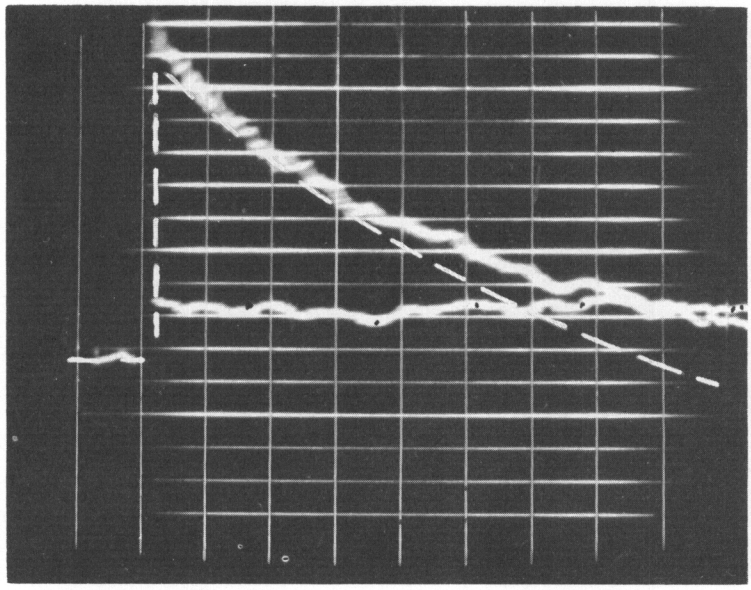

$X_C = 22\frac{1}{4}$"

HORIZONTAL SCALE = 2.5 MILLISECONDS / DIVISION
VERTICAL SCALE = 1 P.S.I. / DIVISION

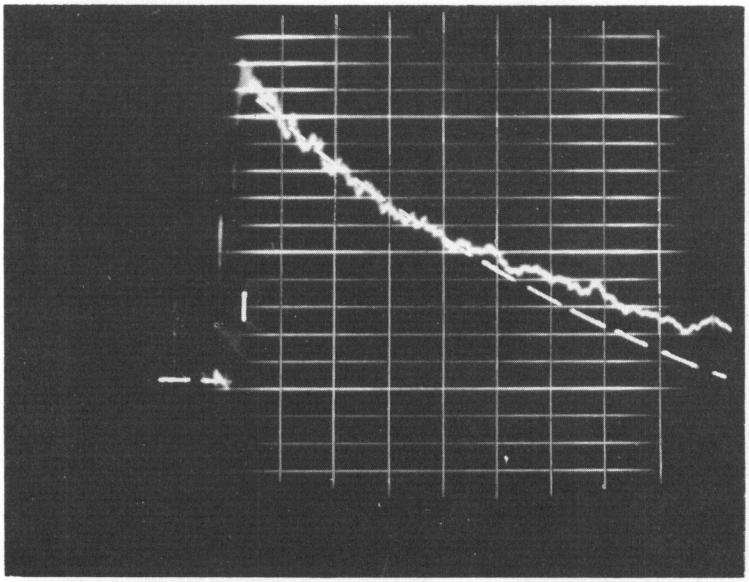

$X_C = 32$"

FIG. 7k MEASURED PRESSURE PROFILES, $p_4 / p_1 = 8.5$

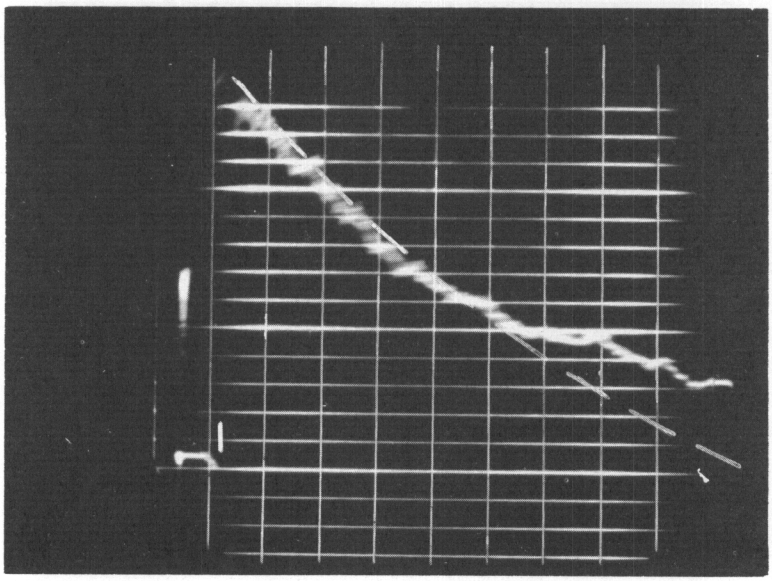

$X_c = 40"$

HORIZONTAL SCALE = 2.5 MILLISECONDS / DIVISION
VERTICAL SCALE = 1 P.S.I. / DIVISION

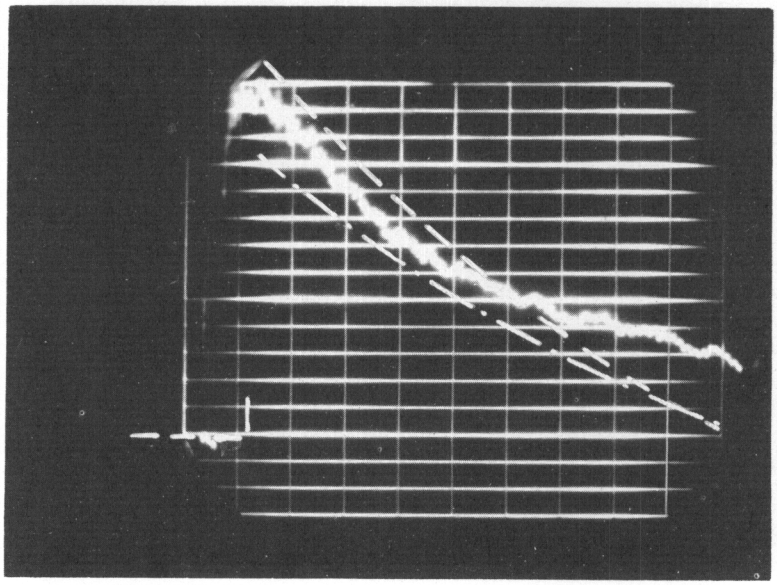

$X_c = 48"$

FIG. 71 MEASURED PRESSURE PROFILES, $p_4 / p_1 = 8.5$

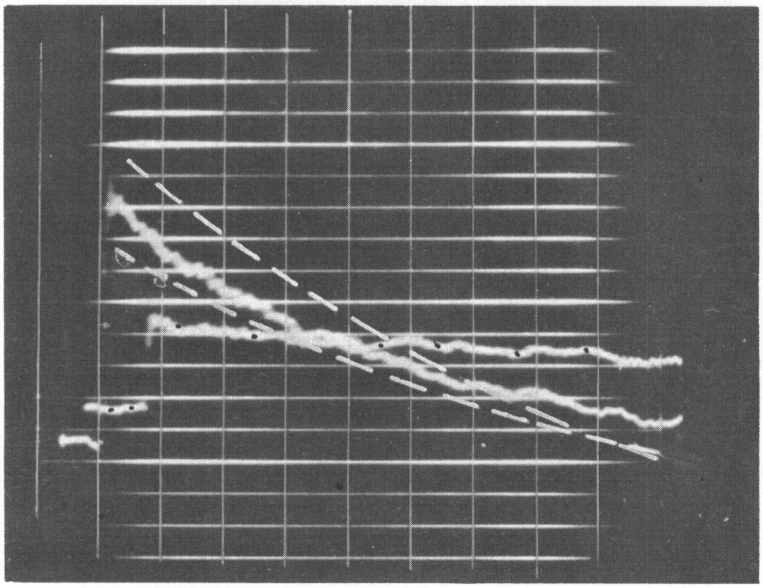

$X_c = 22\frac{1}{4}"$

HORIZONTAL SCALE = 2.5 MILLISECONDS / DIVISION
VERTICAL SCALE = 1 P.S.I. / DIVISION

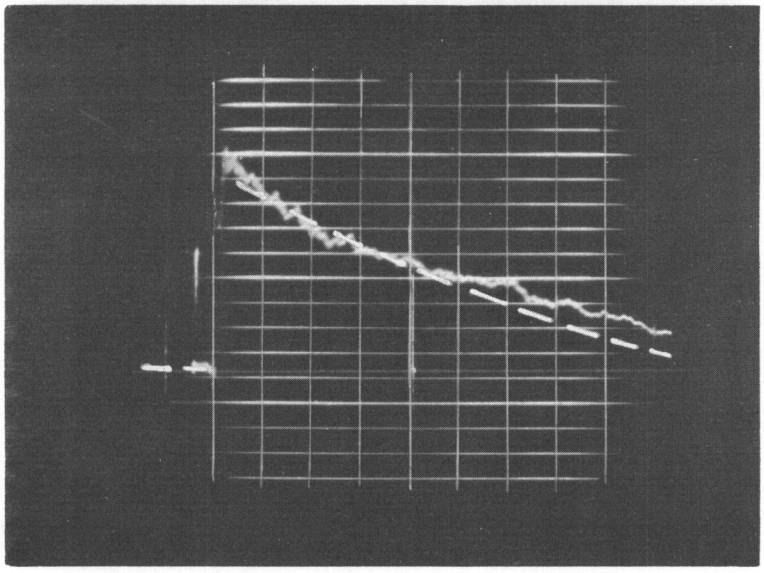

$X_c = 32"$

FIG. 7m MEASURED PRESSURE PROFILES, $p_4 / p_1 = 9.5$

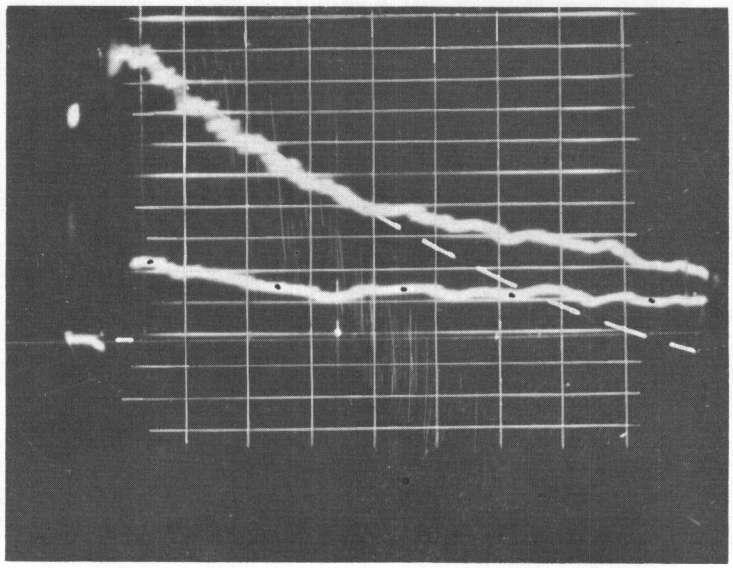

$X_c = 40"$

HORIZONTAL SCALE = 2.5 MILLISECONDS / DIVISION
VERTICAL SCALE = 1 P.S.I. / DIVISION

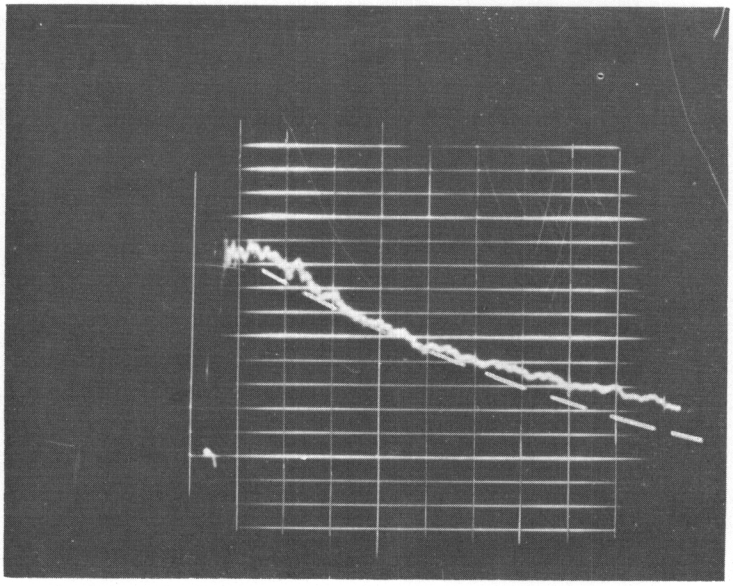

$X_c = 48"$

FIG. 7n MEASURED PRESSURE PROFILES, $p_4 / p_1 = 9.5$

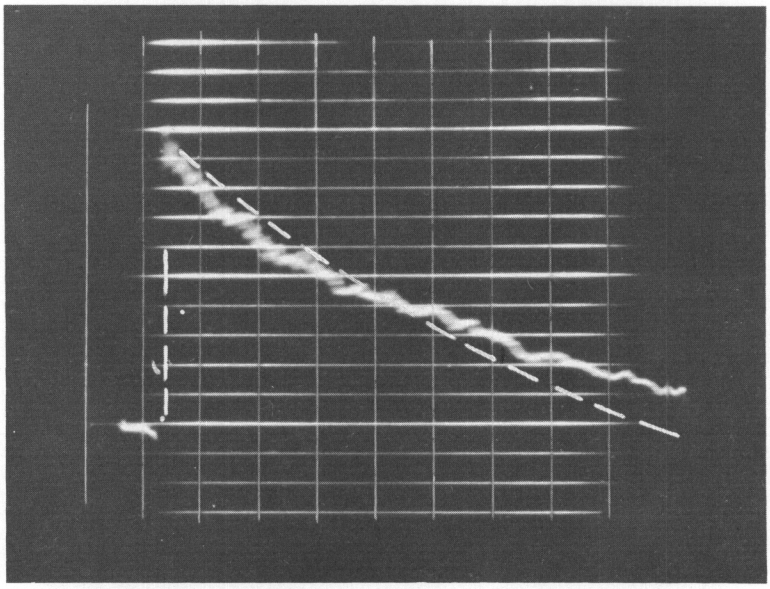

$X_C = 22\frac{1}{4}"$

HORIZONTAL SCALE = 2.5 MILLISECONDS / DIVISION
VERTICAL SCALE = 1 P.S.I. / DIVISION

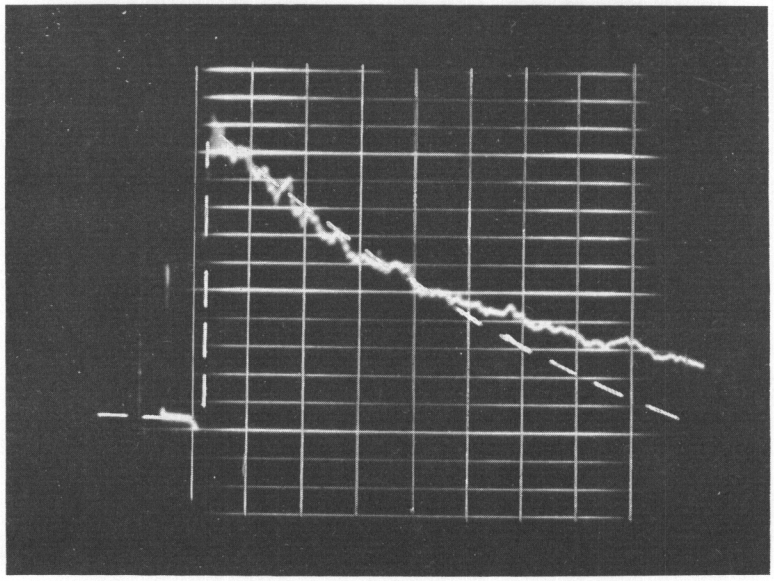

$X_C = 32"$

FIG. 7p MEASURED PRESSURE PROFILES, $p_4 / p_1 = 10.0$

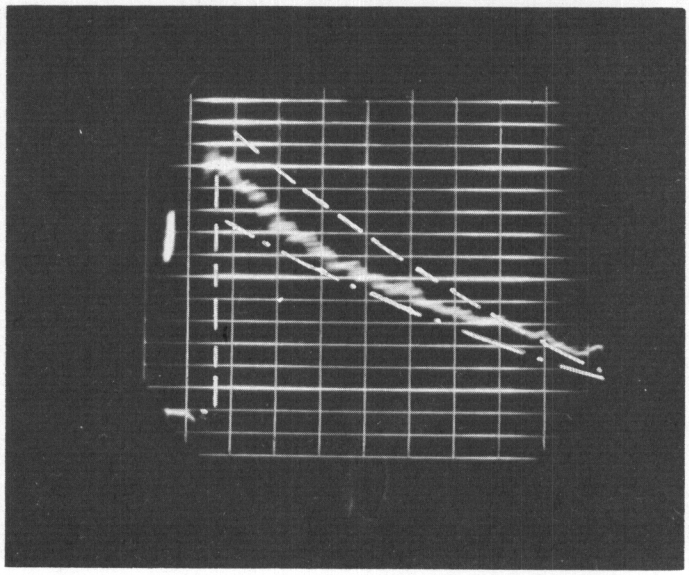

$X_c = 40"$

HORIZONTAL SCALE = 2.5 MILLISECONDS / DIVISION
VERTICAL SCALE = 1 P.S.I. / DIVISION

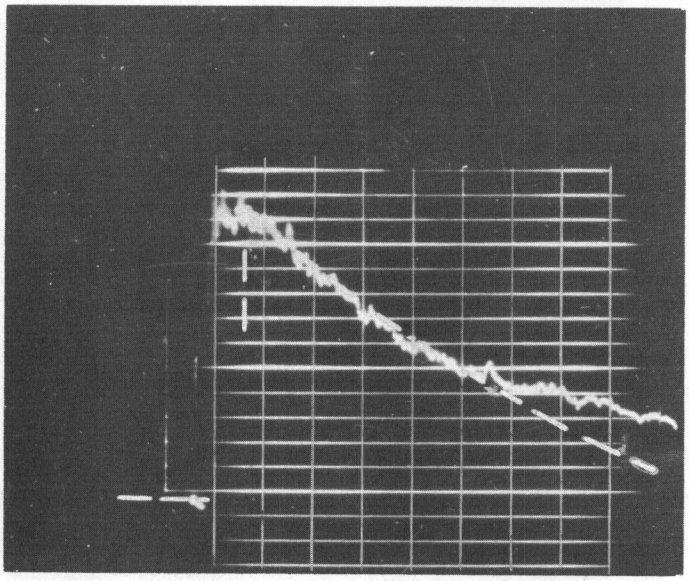

$X_c = 48"$

FIG. 7q MEASURED PRESSURE PROFILES, $p_4 / p_1 = 10.0$

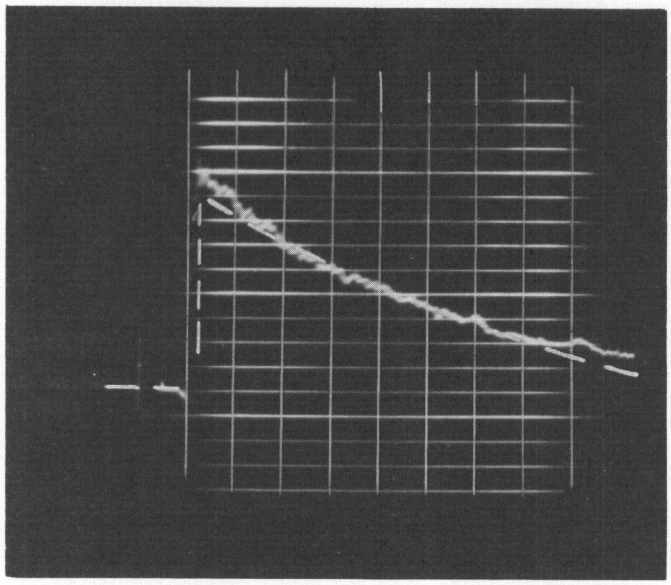

$X_c = 22\frac{1}{4}$"

HORIZONTAL SCALE = 2.5 MILLISECONDS / DIVISION
VERTICAL SCALE = 1 P.S.I. / DIVISION

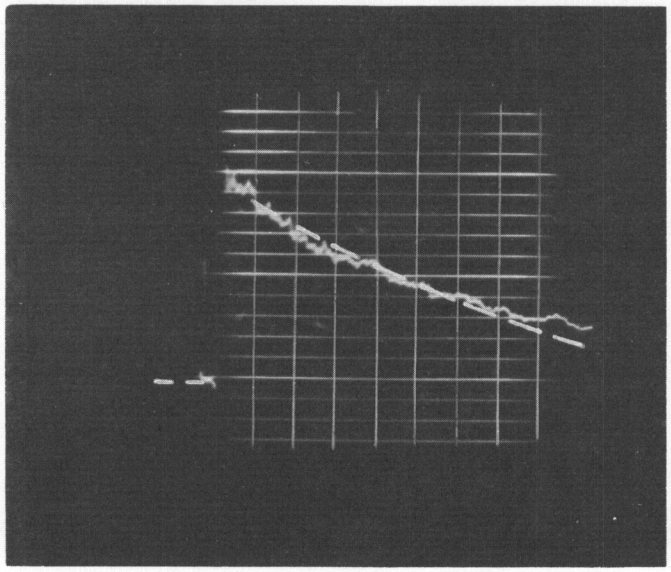

$X_c = 32$"

FIG. 7r MEASURED PRESSURE PROFILES, $p_4/p_1 = 12.4$

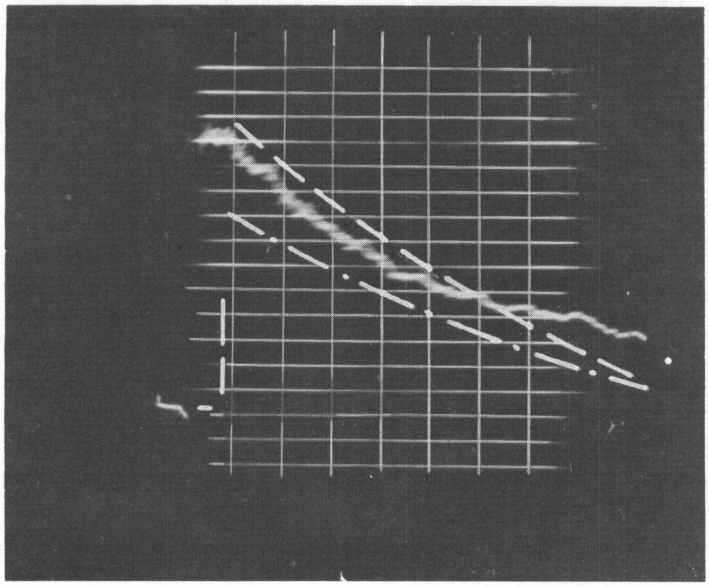

$X_c = 40"$

HORIZONTAL SCALE = 2.5 MILLISECONDS / DIVISION
VERTICAL SCALE = 1 P.S.I. / DIVISION

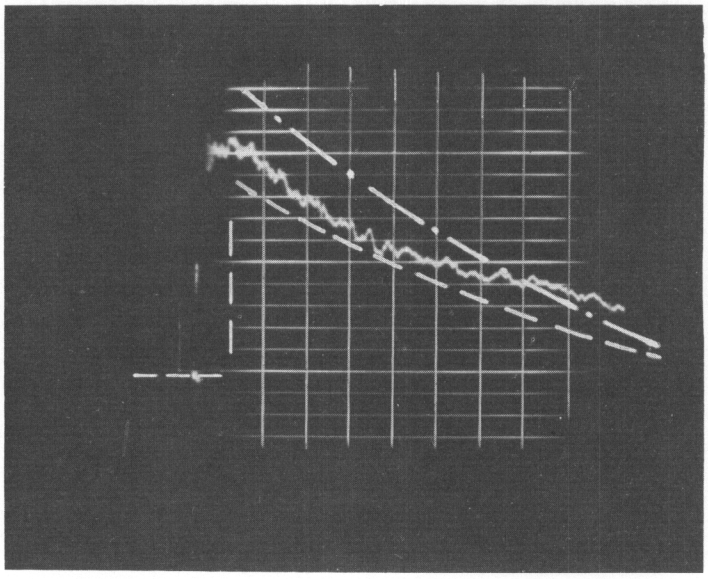

$X_c = 48"$

FIG. 7s MEASURED PRESSURE PROFILE , $p_4 / p_1 = 12.4$

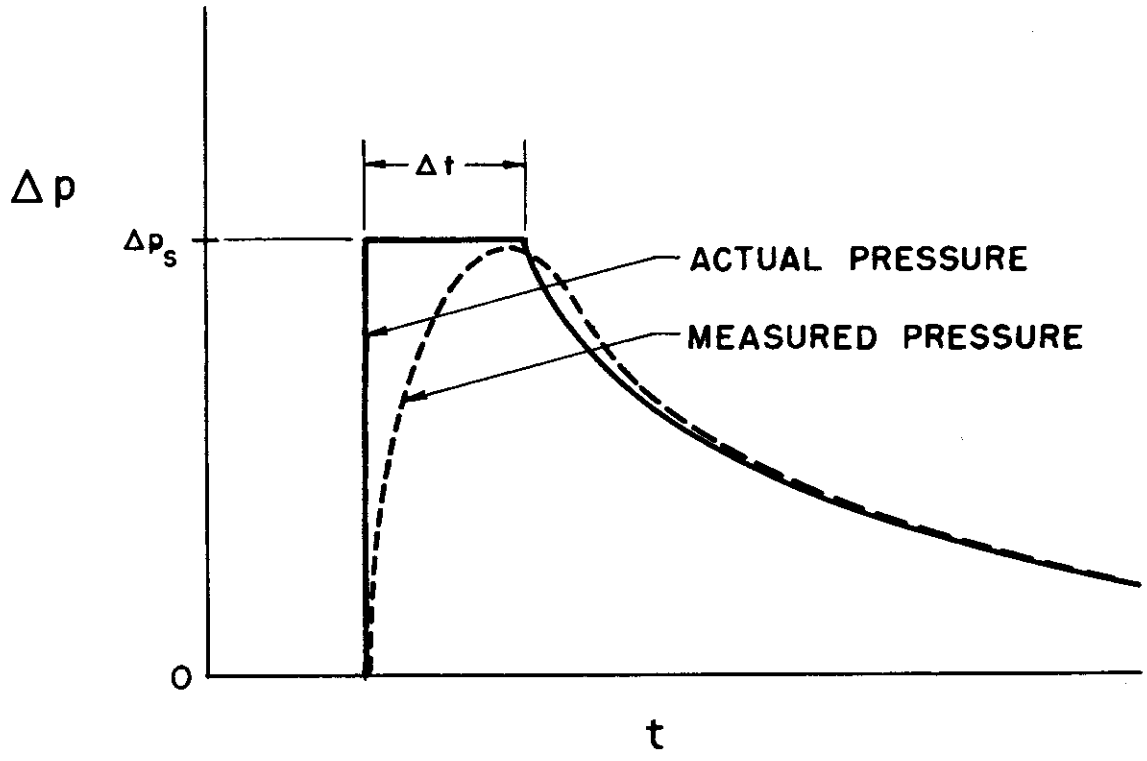

FIG. 8 PRESSURE PROFILE FOR $X_c > X_{c_{OPT}}$ TO ILLUSTRATE SYMBOLS USED

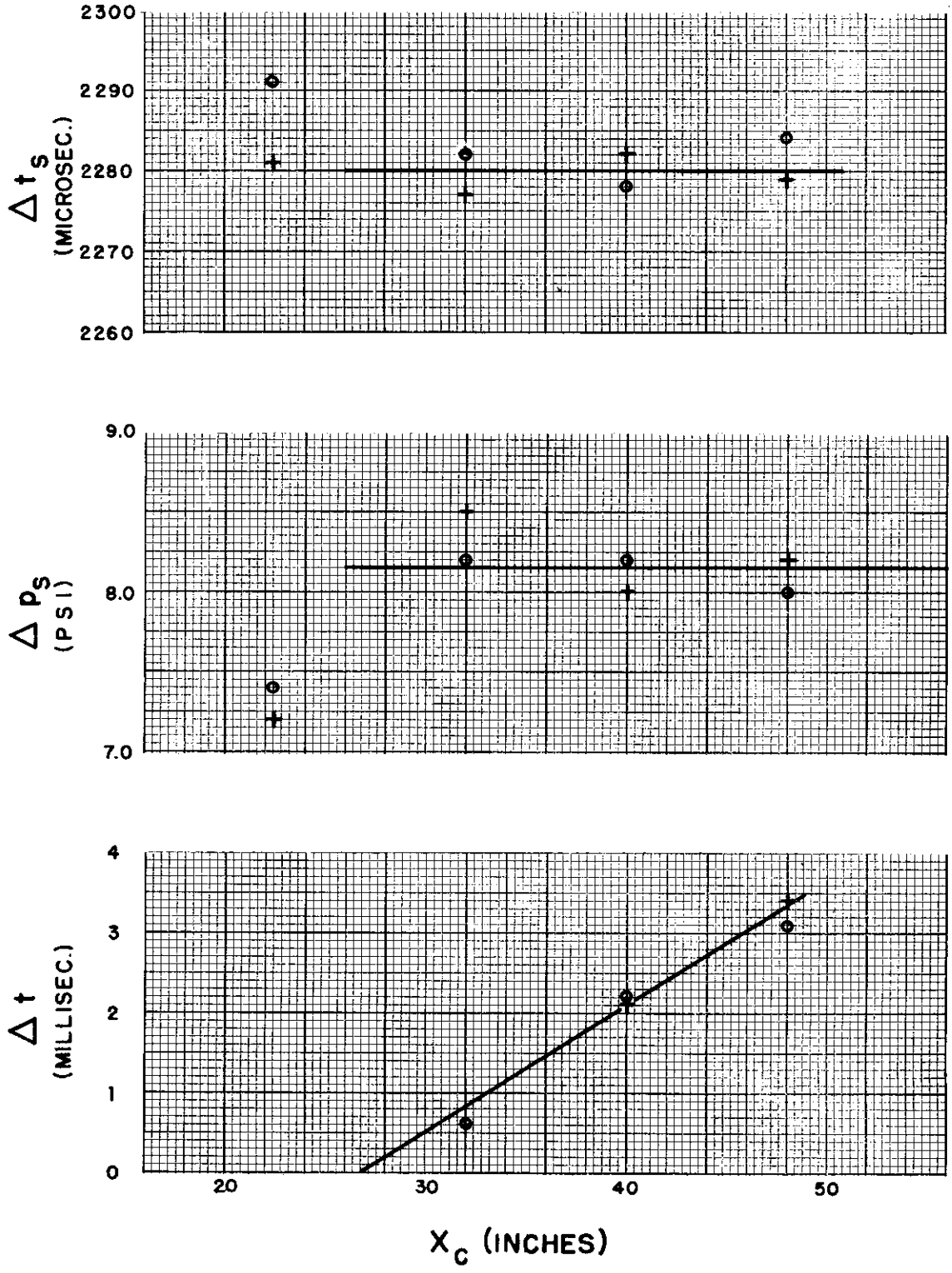

FIG. 9 a VARIATION OF Δt_s, Δp_s and Δt WITH X_c; $p_4/p_1 = 2$

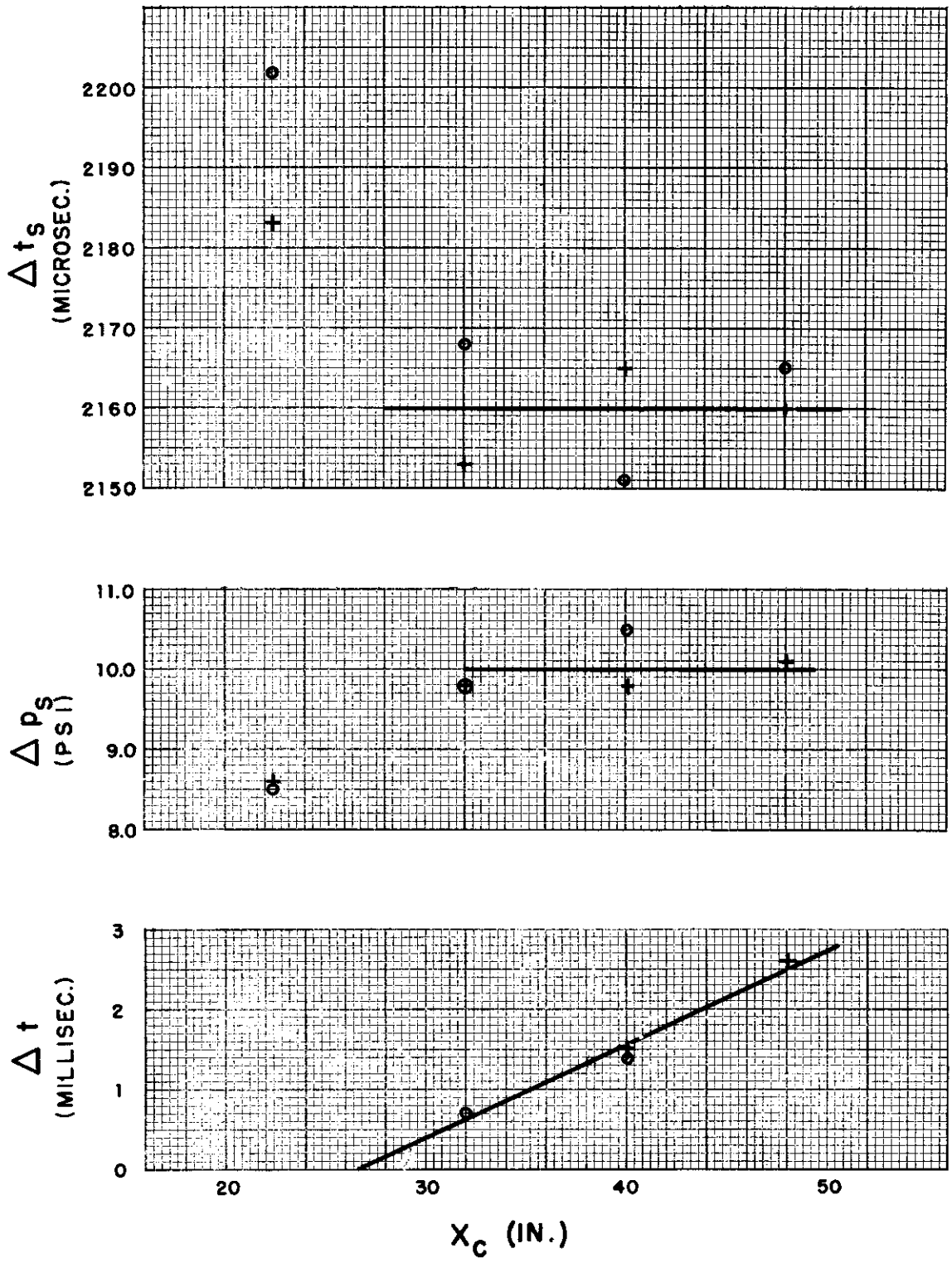

FIG. 9 b VARIATION OF Δt_s , Δp_s and Δt WITH X_c ; $p_4 / p_1 = 2.8$

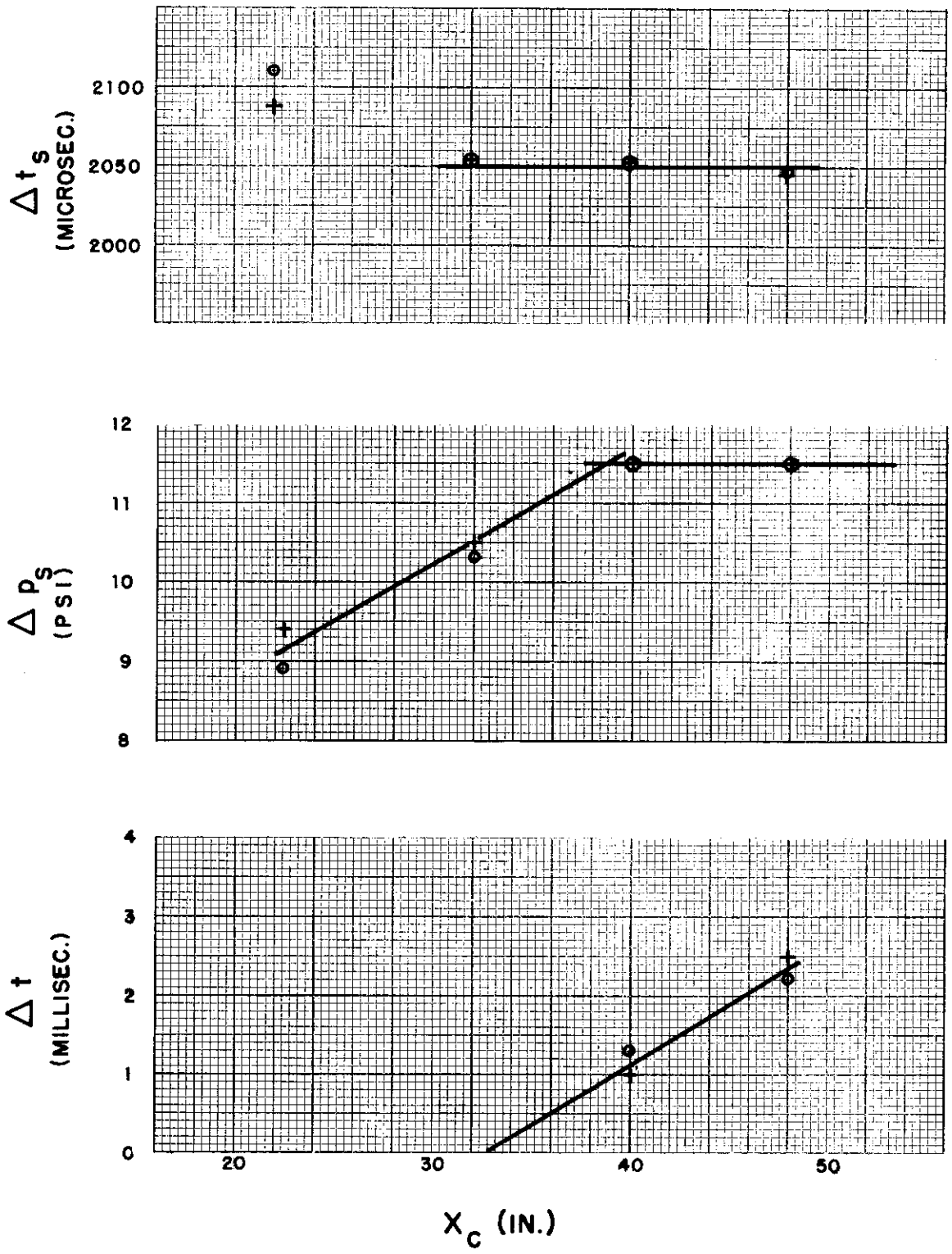

FIG. 9 c VARIATION OF Δt_s, Δp_s and Δt WITH X_c ; $p_4 / p_1 = 3.7$

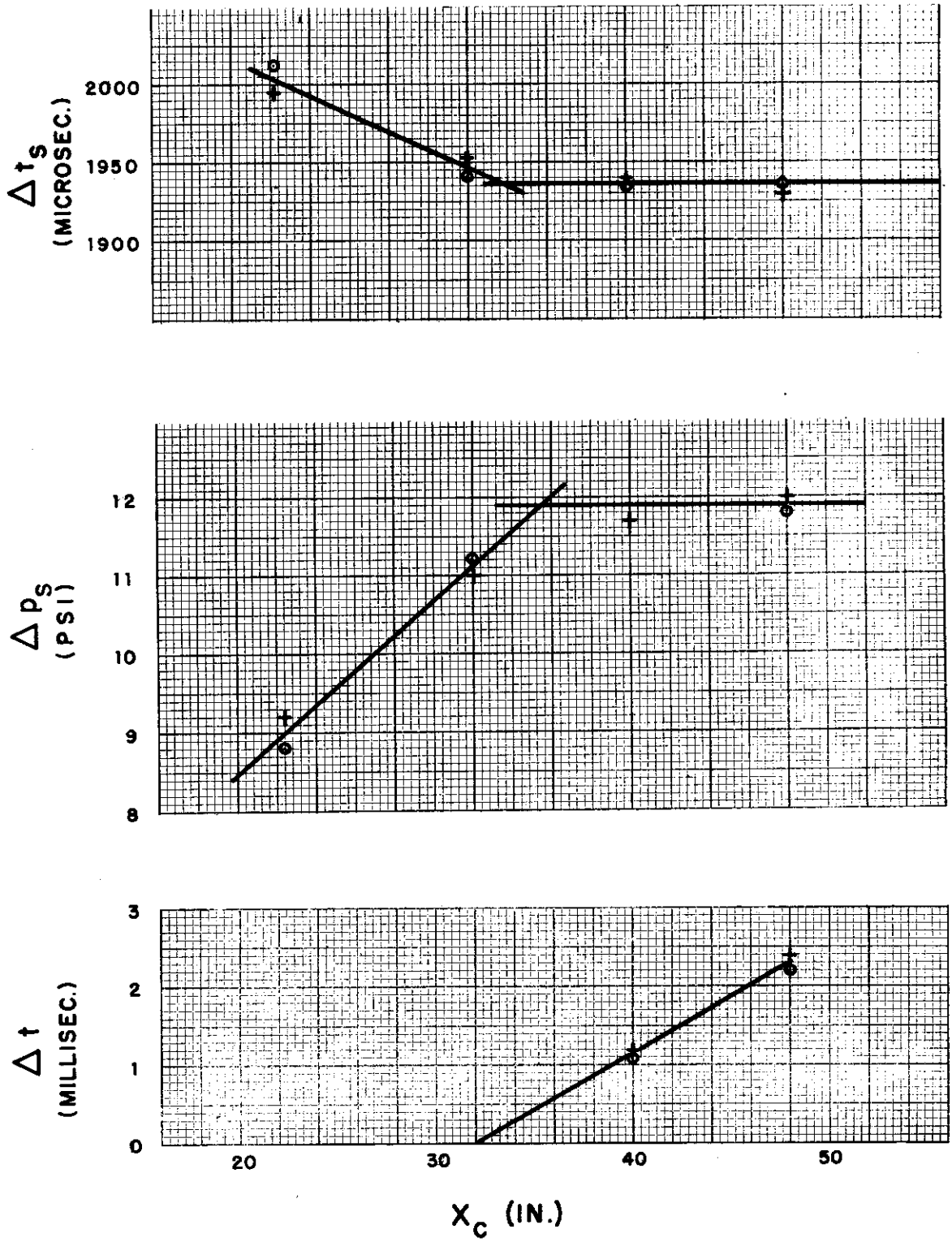

FIG. 9 d VARIATION OF Δt_s, Δp_s and Δt WITH X_c ; $p_4 / p_1 = 5$

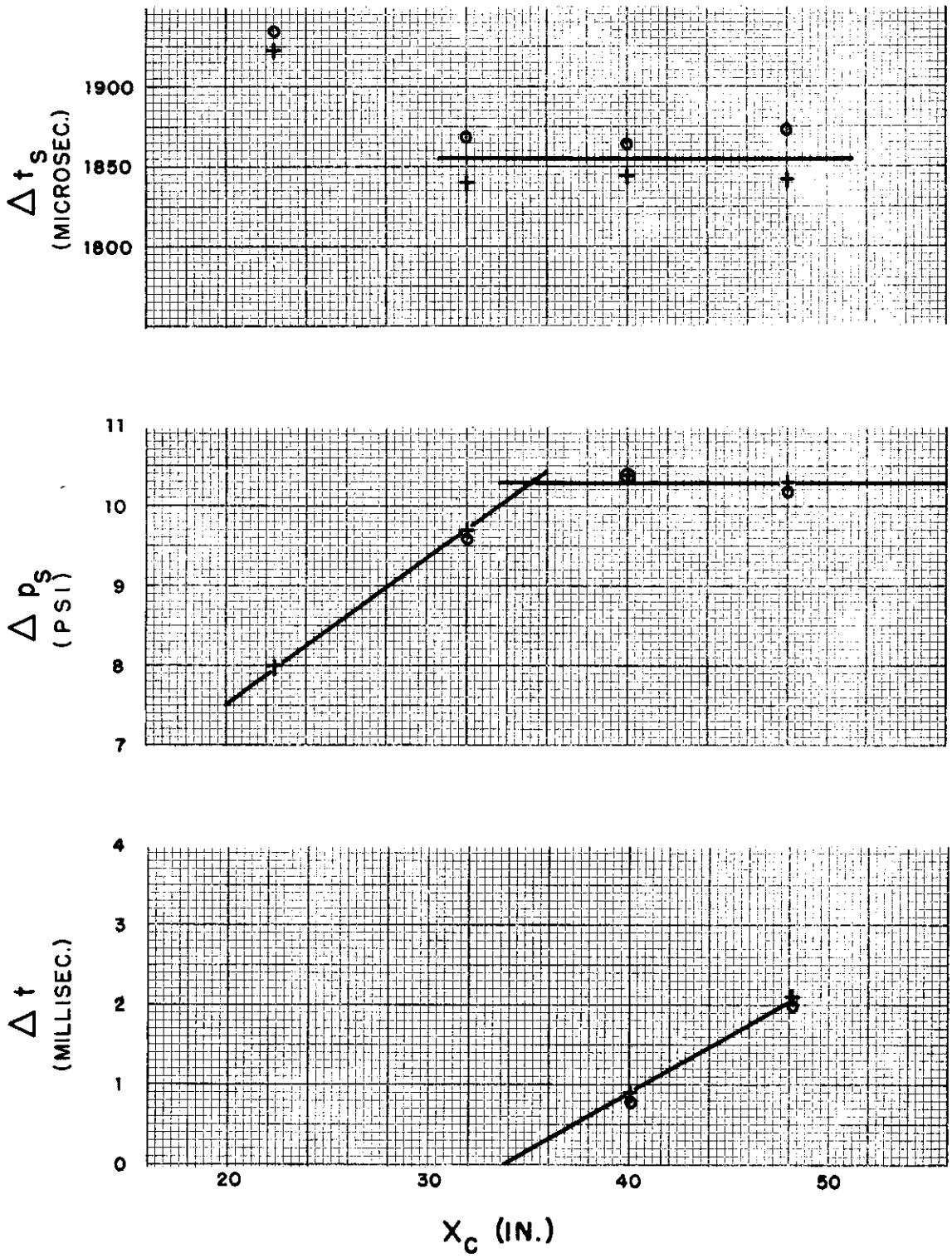

FIG. 9 e VARIATION OF Δt_s, Δp_s and Δt WITH X_c; $p_4/p_1 = 6.2$

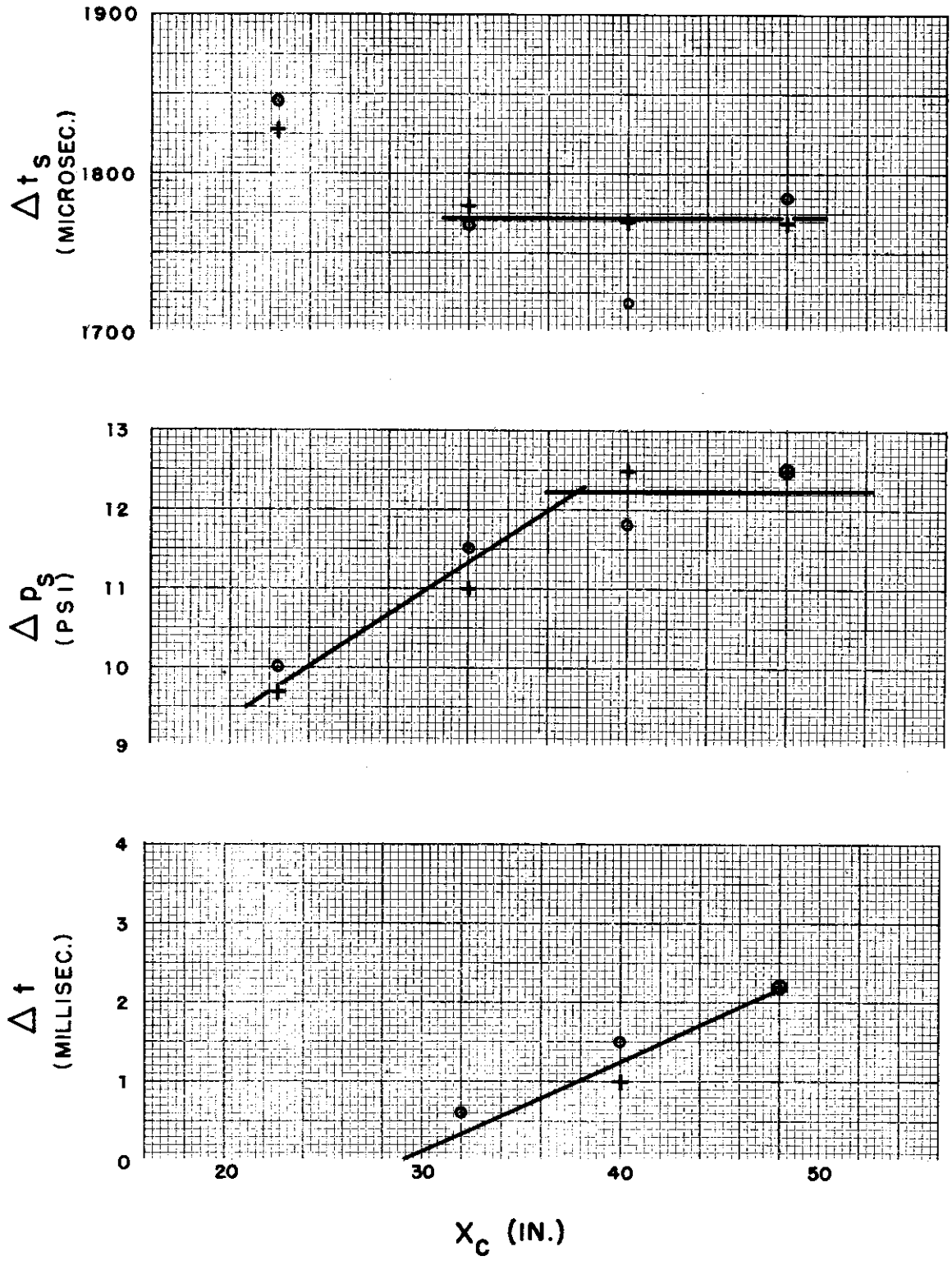

FIG. 9 f VARIATION OF Δt_s, Δp_s and Δt WITH X_c ; $p_4 / p_1 = 8.5$

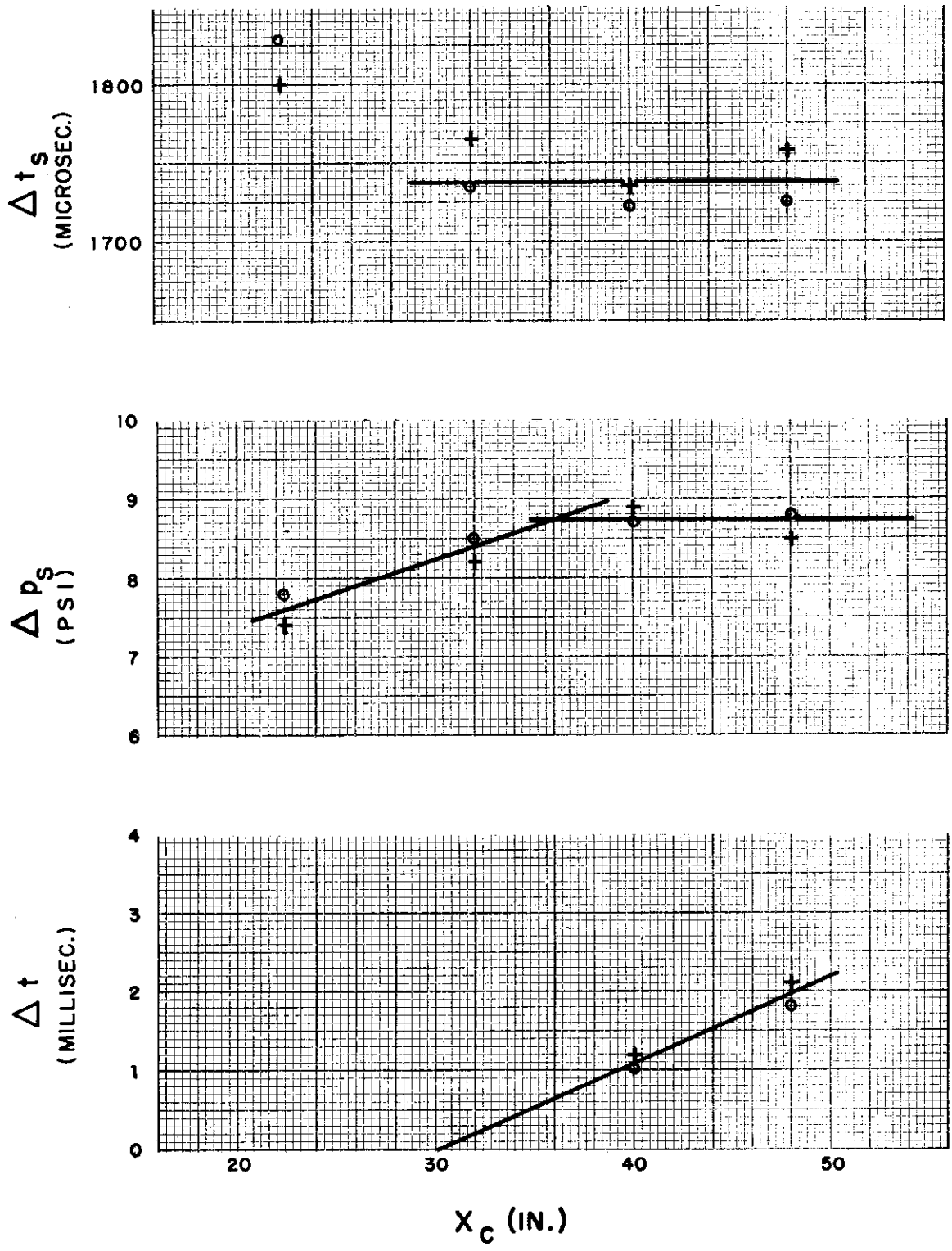

FIG. 9g VARIATION OF Δt_s, Δp_s and Δt WITH X_c; $p_4/p_1 = 9.5$

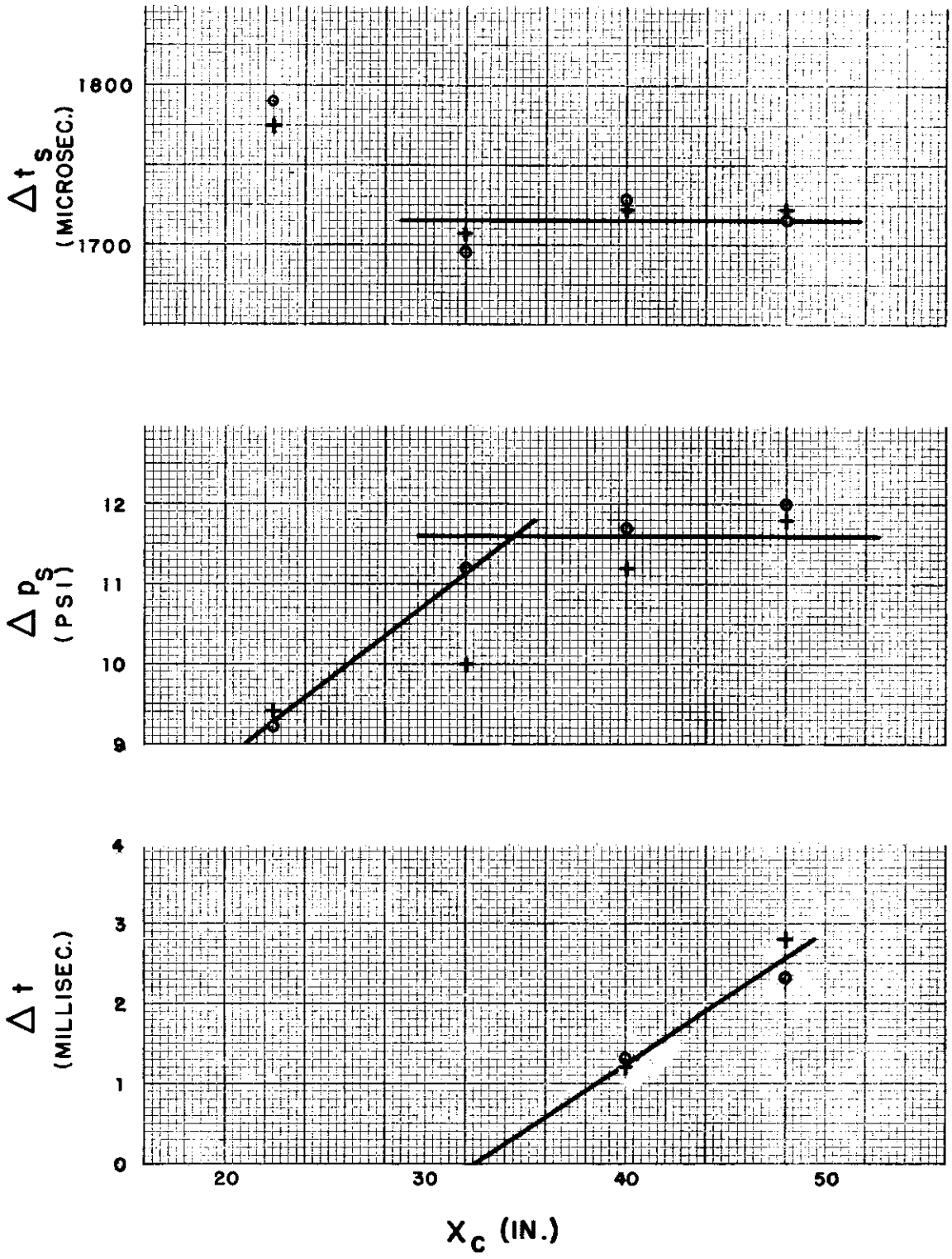

FIG. 9 h VARIATION OF Δt_s, Δp_s and Δt WITH X_c ; $p_4 / p_1 = 10.0$

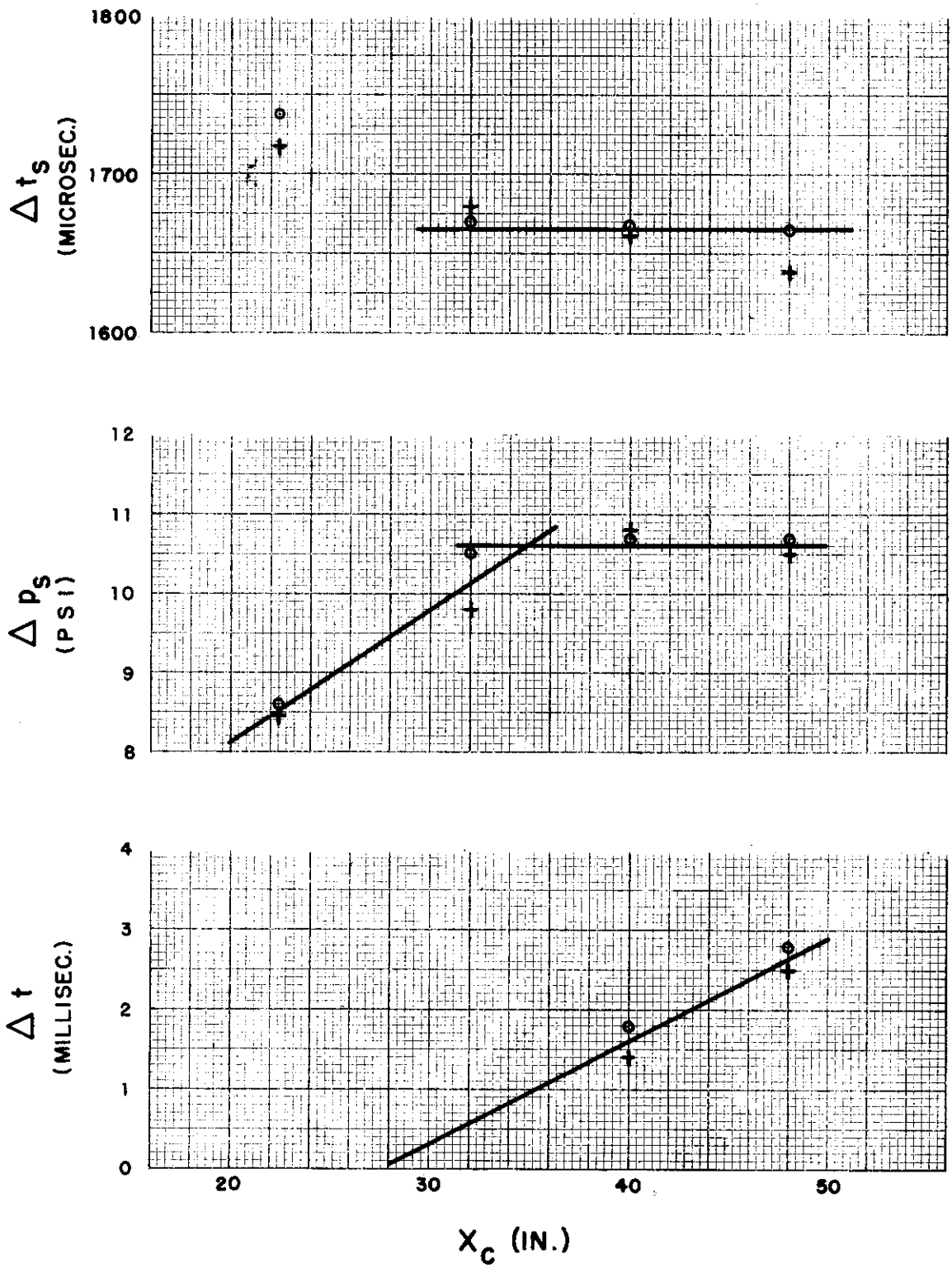

FIG. 9 i VARIATION OF Δt_s, Δp_s and Δt WITH X_c ; $p_4 / p_1 = 12.4$

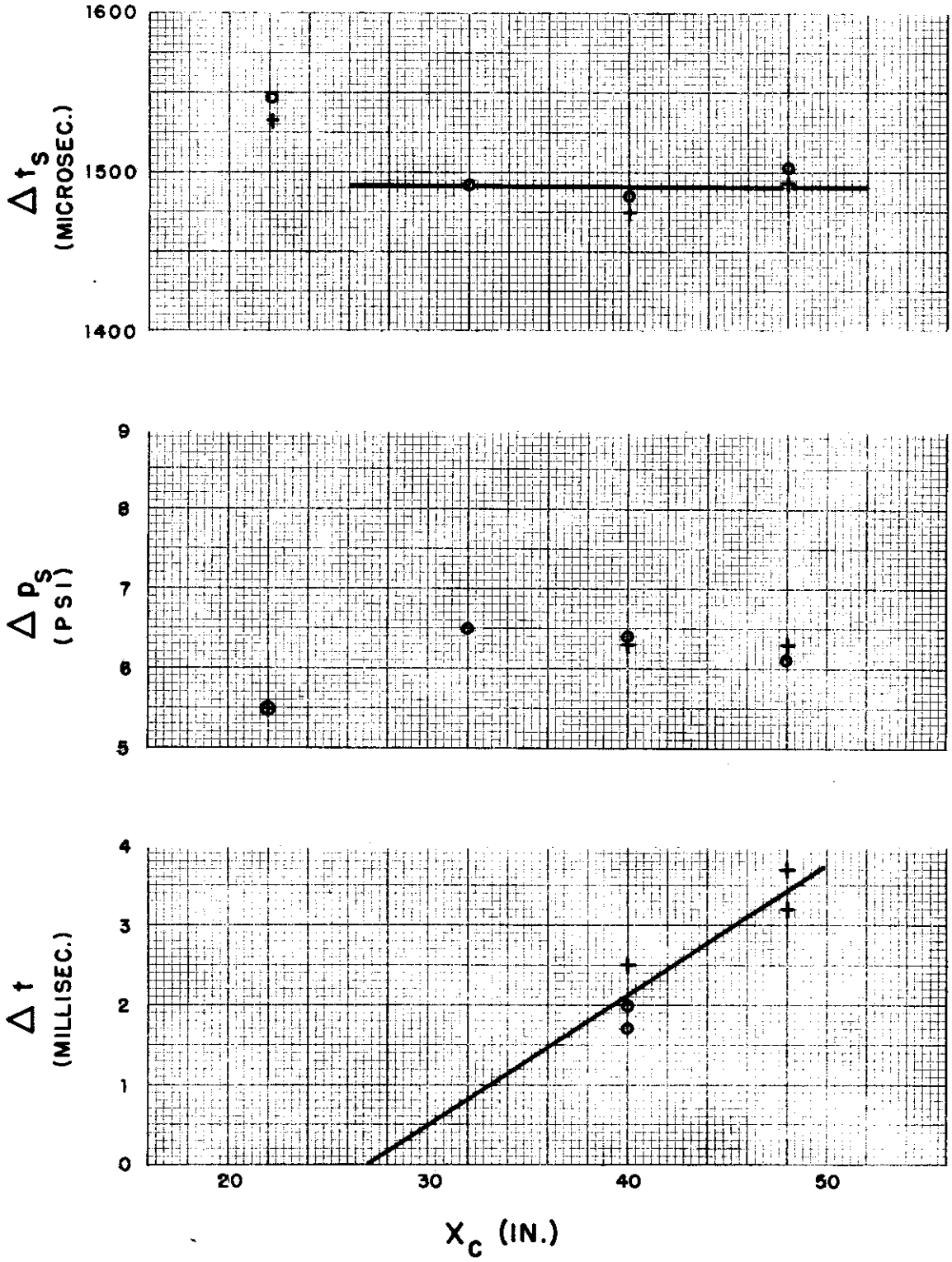

FIG. 9 j VARIATION OF Δt_s, Δp_s and Δt WITH X_c; $p_4 / p_1 = 21.6$

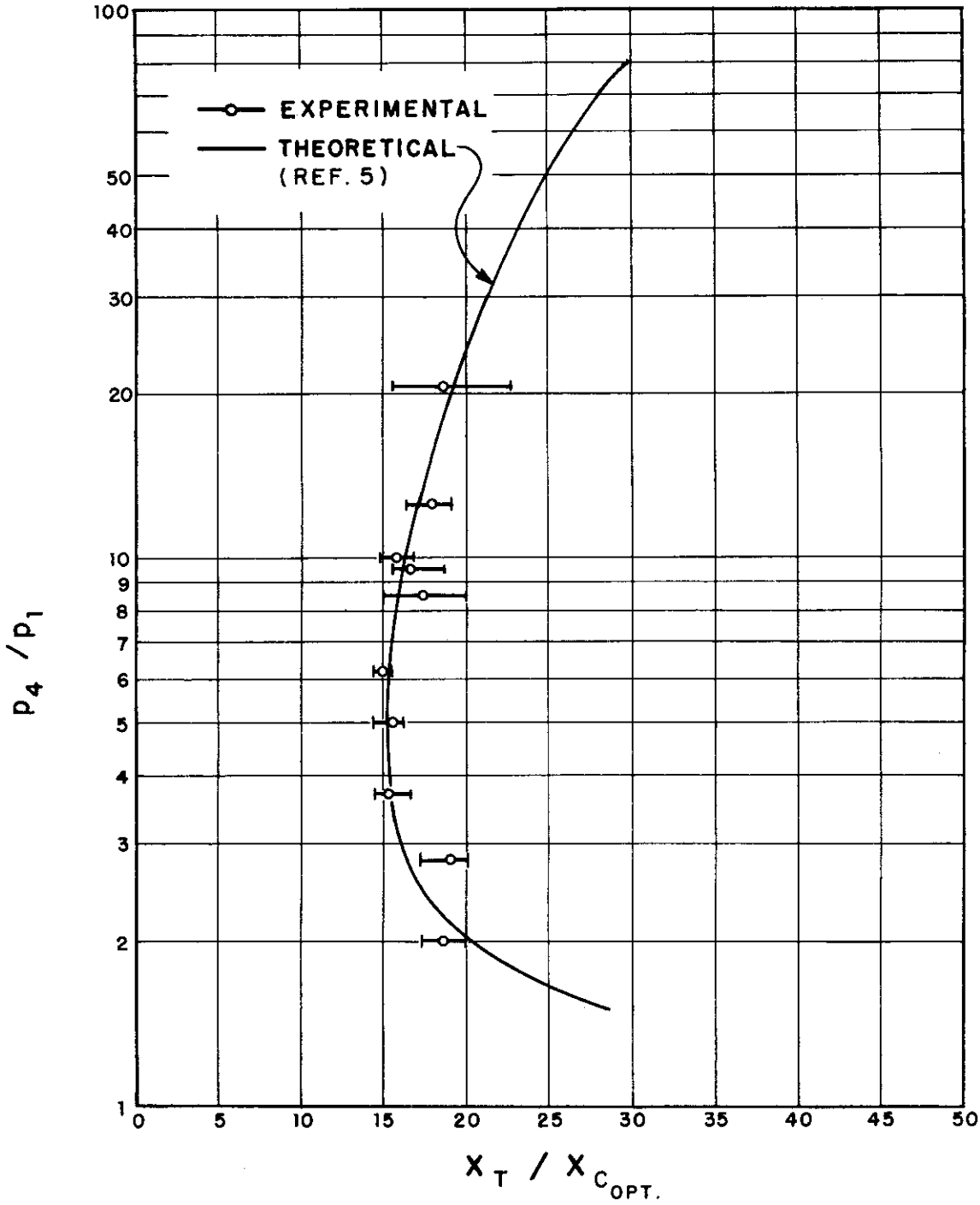

FIG. 10 THEORETICAL AND EXPERIMENTAL VARIATION OF $X_T/X_{C_{OPT}}$ AS A FUNCTION OF p_4/p_1

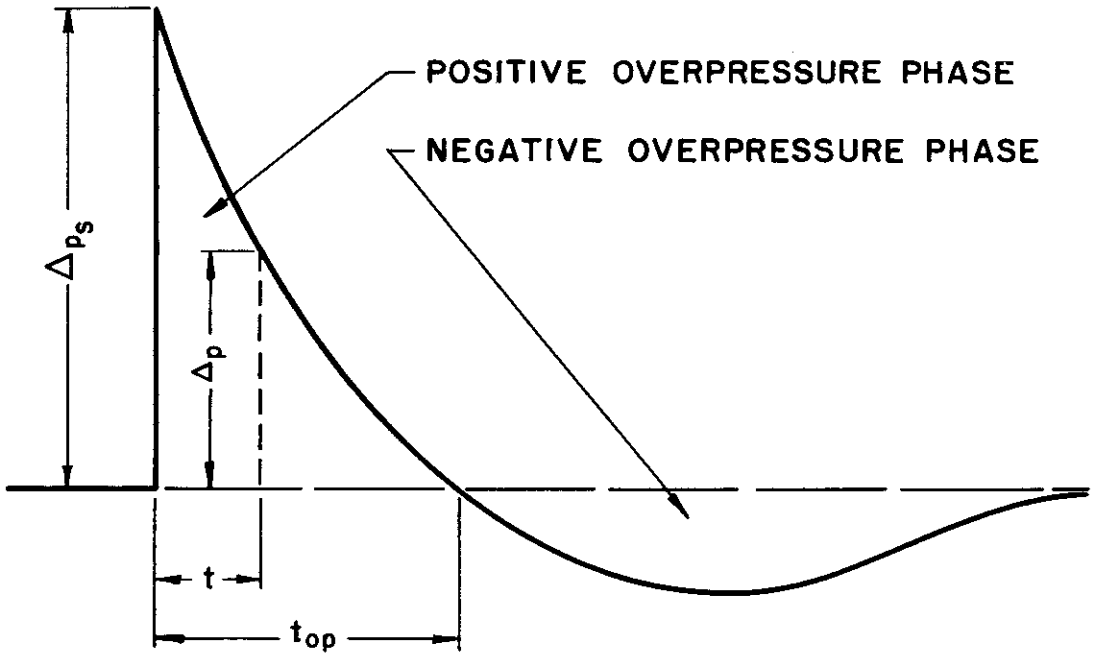

FIG. 11 ILLUSTRATION OF ANALYTICAL BLAST OVERPRESSURE PROFILE

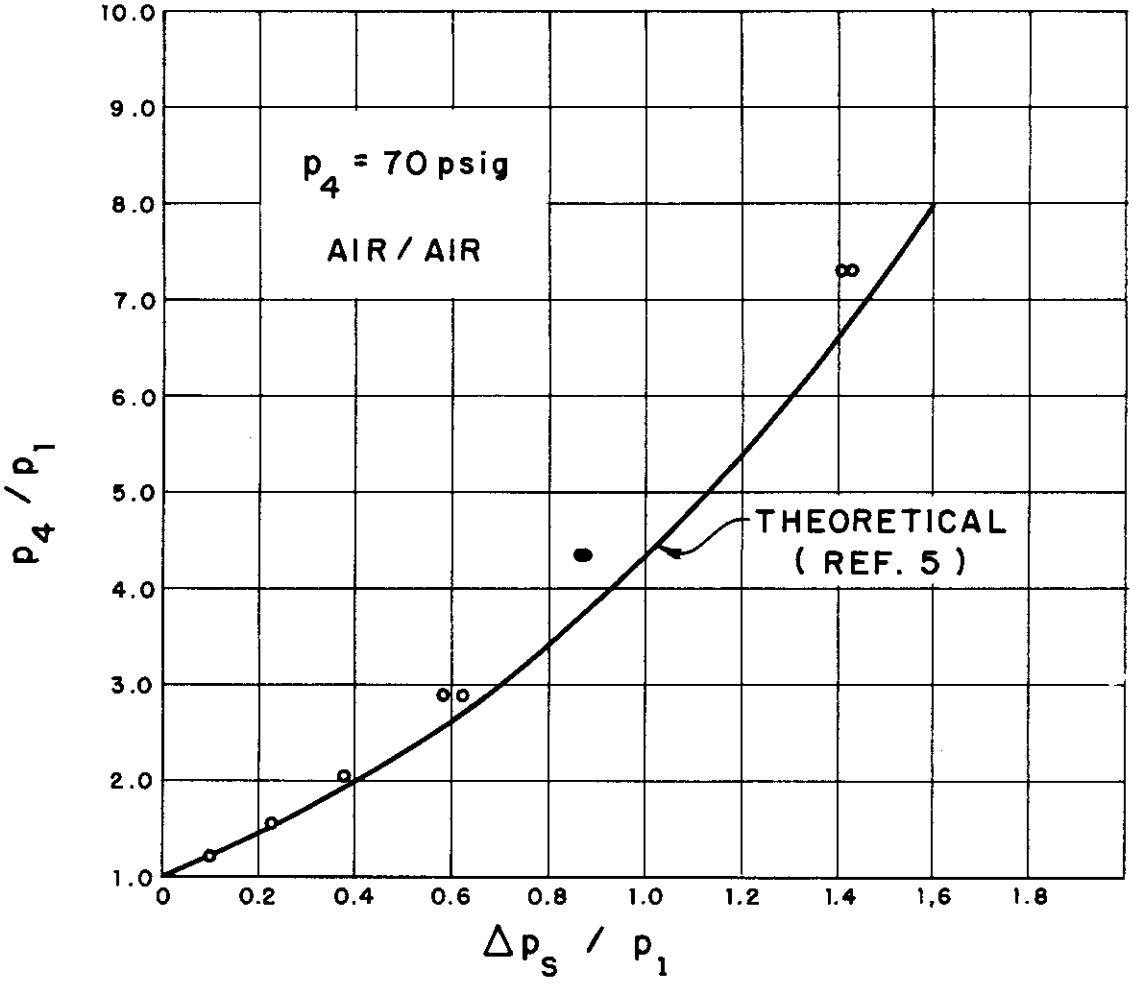

FIG. 12 THEORETICAL AND EXPERIMENTAL VARIATION OF $\Delta p_s / p_1$ VS. p_4 / p_1